Suspended sediment in Quesnel Lake following the Mount Polley Mine tailings spill

by

Brody Granger

B.A.Sc., The University of British Columbia, 2016

A THESIS SUBMITTED IN PARTIAL FULFILLMENT
OF THE REQUIREMENTS FOR THE DEGREE OF

Master of Applied Science

in

THE FACULTY OF GRADUATE AND POSTDOCTORAL STUDIES
(Civil Engineering)

The University of British Columbia
(Vancouver)

June 2020

The following individuals certify that they have read, and recommend to the Faculty of Graduate and Postdoctoral Studies for acceptance, the thesis entitled:

Suspended sediment in Quesnel Lake following the Mount Polley Mine tailings spill

submitted by **Brody Granger** in partial fulfillment of the requirements for the degree of **Master of Applied Science** in **Civil Engineering**.

Examining Committee:

Bernard Laval, Civil Engineering Engineering
Supervisor

Svein Vagle, Institute of Ocean Sciences, Fisheries and Oceans Canada
Supervisory Committee Member

Abstract

In the four years that followed the 4 August 2014 tailings dam failure at Mount Polley Mine, British Columbia, Canada, water quality data indicated an ongoing sediment loading to Quesnel Lake and the Quesnel River. Within one day of the tailings dam failure, a flood of slurry entered the smaller, downstream basin of Quesnel Lake, called the West Basin. Previous studies had shown highly elevated turbidity in the West Basin through the first autumn and winter after the spill, and above background turbidity each autumn and spring from 2015 onwards. It remained unclear how long this seasonally elevated turbidity would last. In this thesis, we evalutate sediment transport in Quesnel Lake following the rapid inflow of a vast quantity of material. This thesis applies conservation of mass in two ways: first, using data collected between 10 September 2014 and 21 December 2018 to estimate suspended sediment mass and mass flows into and out of the West Basin; and second, using an analytical model. On 10 September, 37 days post-spill, an estimated 38000 ± 11000 Mg of solids remained suspended in the West Basin; this decreased to within background levels ($<$300 Mg) by early June 2015. Between 10 September 2014 and 3 June 2015, 4000 ± 1200 Mg of sediment flowed from the West Basin into the Quesnel River, and ~ 31000 Mg entered the main basin of Quesnel Lake. A gradually decaying, seasonal cycle emerged thereafter: near background each summer, somewhat elevated during winter and spring, and above background each autumn, with an interannual decrease in magnitude. Remobilization of a turbid, bottom layer by internal wave motions during each autumn of 2015-2018 contributed to an increased mass of suspended sediment in the West Basin. Together with the observed mass trend, an analyticial mass balance model of a simplified, two basin system suggests a return to background suspended sediment levels by one decade post-spill.

Lay Summary

The largest accidental spill of mining waste that has occurred to date in Canada began in the early morning on 4 August 2014, at Mount Polley Mine, a copper and gold mine located in central British Columbia. Within the day, nearby Quesnel Lake received a volume of waste roughly equivalent to 2% of the volume of its smaller, downstream basin, the West Basin, where the spill entered the lake. In this study, we evalutated the movements of fine sediment in Quesnel Lake and the Quesnel River using water quality data collected between 10 September 2014, 37 days post-spill, and 21 December 2018. We then developed a simplified, two basin model based on mathematical theory which broadly decribes the response of Quesnel Lake's two basins, and used this to estimate that suspended sediment will have returned to background levels ten years after the spill.

Preface

For consistency, I have used the pronoun *we* throughout the text. In many cases, my use of *we* acknowledges that there are individuals whose contributions made this study possible, especially in regard to the enormous undertaking of data collection that continues in the Quesnel Lake and River system. I developed this thesis under the guidance of my supervisor and mentor in physical limnology, Dr. Bernard Laval, who is the first coauthor listed on the manuscript-in-preparation that has come out of this work. Dr. Svein Vagle, the second coauthor listed as well as my second thesis committee member, has been a key contributor to the design and servicing of the moorings and has provided useful feedback at many stages of this work's development. As well, I have received helpful comments and suggestions on the text from two further coauthors: Dr. Philip N. Owens, and Dr. Ellen L. Petticrew. They oversaw and participated in collection of the CTD data used in this study, along with staff at the University of Northern British Columbia's Quesnel River Research Centre in Likely, BC. Dr. Andrew K. Hamilton offered me a valuable opportunity to collaborate as a coauthor of a companion study to this thesis which has recently been accepted for publication in the journal *Water Resources Research*, and gave me a leg up in processing CTD data.

In other cases, the use of *we* is misleading. The data analysis, reasoning, and writing contained herein are my own.

Table of Contents

List of Tables

List of Figures

Acknowledgements

Thank you to the staff at the Quesnel River Research Centre: Sam Albers, Michael Allchin, Laszlo Enyedy, Todd French, Caitlin Langford, Ido and Jordan Lindgren for providing technical assistance in the field, and especially for collecting CTD data; to all those who helped service the moorings: Kelly Graves, Sam Brenner, Lydia Smith, Sarah Chang, and Jérémie Bonneau; to fellow researchers Ido Hatam and Susan Baldwin for helping to bring the slocores ashore; to Mount Polley Mining Corporation for CTD data from the first post-spill fall, winter, and spring; and to Environment and Climate Change Canada, both for making environmental data available online, and for providing financial support through the Environmental Damages Fund.

To my parents, Cheryl and Clive, thanks for giving me a place to stay and home cooked meals on my way to and from field work (as well as through my whole upbringing).

Chapter 1

Introduction

The presence of suspended sediment in lakes is often apparent in the color and clarity of the water (Bloesch, 1995). Oligotrophic lakes contain predominantly minerogenic particles, such as silts and clays (Håkanson and Jansson, 1983); with less abundant organic (i.e., low loss on iginition) and inorganic, biogenic particles (Wetzel, 2001a). Higher suspended sediment concentration leads to more light scattering and absorption, which alters primary productivity by limiting the depth of the photic zone, and modifies the distribution of heat from incoming solar radiation (Valipour et al., 2017; Wetzel, 2001b). Where nutrients or pollutants are associated with sediment, changes in concentration can have ecological effects (Håkanson and Jansson, 1983). Riverine inflows are typically the main source of allochthonous (from the drainage basin, carried into the lake) sediment (Scheu et al., 2015), as is the case with the glacial flour that gives many mountain lakes their turquoise color. Lake Winnipeg provides two examples of autochthonous (from within the lake) sediment: decaying organic matter produced by vast, green algal blooms; and brown silt and clay resuspended from the bottom in shallow regions during strong winds (Schindler and Vallentyne, 2008).

In deeper regions, below the oscillatory motions of surface waves, currents resulting from basin-scale internal waves (seiche) can resuspend sediment (Bloesch, 1995; Gloor et al., 1994, 2000; Valipour et al., 2017). Internal seiching occurs during stratified periods when sustained wind-forcing tilts the density interface. Gravity acts to restore this tilt, and the lake becomes a mechanical oscillator damped mainly by bottom shear stress (Wüest et al., 2000), which in turn creates a turbulently

mixed benthic boundary layer (Marti and Imberger, 2006). Most seiche damping (and its associated turbulence) occurs where lake bathymetry interacts with the density interface, for example constrictions between basins, or the sloping bottom region around a basin (Chowdhury et al., 2016; Lawrence et al., 1997). Benthic matter that is entrained by these flows is mixed along with heat to form uniform, localized parcels of fluid. Depending on the density of this fluid, it may flow to the bottom as a turbidity current, or sink to a level of neutral buoyancy within the background density gradient. From there, it will collapse radially into the lake's interior as a lens-like, horizontal intrusion (Wain and Rehmann, 2010).

On 4 August 2014, a breach in the perimeter embankment dam surrounding the tailings storage facility at Mount Polley Mine, a copper and gold producer in central British Columbia, Canada, released 25 million m^3 of waste solids and water into the surrounding environment (MPMC, 2015). Within one day of the breach, ~20 M m^3 of tailings, scoured surficial material, and water (both interstitial and supernatant) entered the West Basin of Quesnel Lake (Figure 1.1). While most of the solids settled quickly to the bottom where they formed a several meter thick deposit, an appreciable mass of fine sediment remained in suspension (on the order of 10 Gg in early October 2014, nearly all of it below 35 m depth, roughly the depth of the density interface; Petticrew et al., 2015).

To date, no peer-reviewed report has provided a detailed account of the fate of this sediment in Quesnel Lake and the Quesnel River, in British Columbia's Fraser River catchment. Attempts to numerically model Quesnel Lake following the spill have produced estimates of how much spill-related sediment flowed into the Quesnel River and the main basin of Quesnel Lake (Tetra Tech EBA, 2015). Given the limited data used to verify the model, the relability of these estimates is questionable.

The Mount Polley spill was a unique case: a slug injection of mine waste into a comparitively small, downstream basin in a two basin lake (the term *slug injection* describes a single, effectively instantaneous release of substance.) Theory suggests that in a two basin system, the response to a slug injection of sediment will be two-phased: initial, fast decay of mass giving way to long-term, slow decay (Chapra, 1997). Earlier work by Hamilton et al. (2020), described in Chapter 2, has similarily shown that the amount of sediment in the West Basin through most of the first

year post-spill was significantly larger than in the second and third years post-spill. Our sediment transport observations (Chapter 4) are presented in two sections which correspond to the two phases predicted by theory and observed in the West Basin: section 4.1, where we have paid particular attention to the relative importance of three sinks (river, lake bottom, and main basin) in removing suspended sediment mass from the West Basin; and section 4.2, where we assess these three sinks as well as sediment sources, notably the influence that seiche-driven bottom dynamics had on the apparent sediment loading to the hypolimnion of the West Basin each autumn of 2015-2018. Lastly, in Chapter 5, we assess the long-term recovery trend using an analytical mass balance model, and discuss the implications for suspended sediment, as well as other pollutants, discharged into Quesnel Lake.

1.1 Study site

Quesnel Lake (volume: 41.8 km^3, surface area: 266 km^2), shown in Figure 1.1, inset (ii), extends from the foothills of the Cariboo Plateau into the Cariboo Mountains of central British Columbia, Canada. Viewed on a map oriented east-up, the lake's three arms resemble a lowercase "y". At a maximum depth of 512 m (Gilbert and Desloges, 2012), it is the deepest fjord lake in Canada and the third deepest lake in North America. Like most fjord lakes, it is long (east-west thalweg length: 95 km), narrow (mean width: 2.7 km), and has multiple basins (two). The West Basin (volume: 1 km^3, surface area: 22 km^2) is the hook at the bottom of the lowercase "y" (Figure 1.1, main panel). It curves from a westerly to a northerly orientation over 20 km, broadening and deepening from a 35 m sill near Cariboo Island to its deepest section offshore of Hazeltine Creek, then becoming shallow and narrow towards the outflow. Its maximum depth prior to the spill was 121 m (Gilbert and Desloges, 2012); the spill decreased this to 108 m (MPMC, 2015). Near the town of Likely in the northernmost reach of the West Basin, Quesnel Lake drains into the Quesnel River (mean annual flow = 131 m^3/s; Laval et al., 2012).

The 4 August 2014 spill entered the West Basin via Hazeltine Creek (Figure 1.1, main panel). Mount Polley Mine's location to the west of the West Basin is shown in Figure 1.1, inset (ii). The mine's tailings storage facility is located about 9 km upstream and 200 m above the small delta

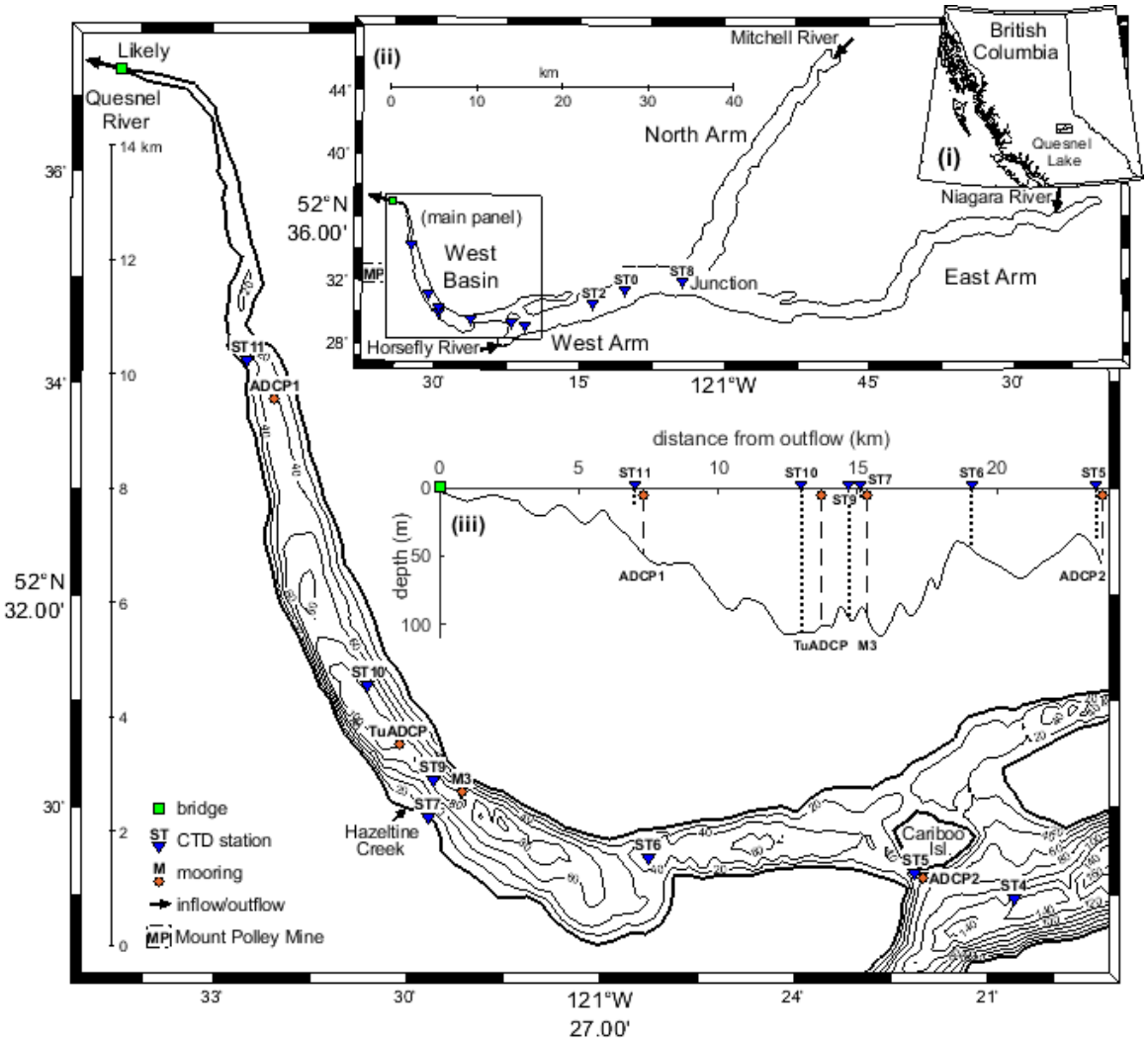

Figure 1.1: Map of West Basin with 20 m depth contours. Inset (i) shows the location of Quesnel Lake in British Columbia, inset (ii) shows the location of the West Basin in Quesnel Lake, and inset (iii) is an along-thalweg depth plot for the West Basin indicating locations of CTD stations and moorings (also indicated in main panel). Note that ST11 and ST7 have shallow cast depths indicated by dotted lines in (iii), as these two are located near shore.

where Hazeltine Creek drains into the West Basin. By 1 December 2015, Mount Polley Mine had diverted the flow of Hazeltine Creek into two settling ponds which discharged runoff, along with mine effluent, through diffusers at 40 m depth in the West Basin until 30 September 2017 (MPMC, 2018). From that date onward, the mine piped effluent directly to the diffusers and reestablished the Hazeltine Creek inflow at the shoreline.

Chapter 2

Literature Review

By the 1950s, limnologists and sedimentologists had begun to apply conceptual and mathematical models to describe sediment transport in lakes (Håkanson and Jansson, 1983). Increasing attention has since been given to the science of lake sediment transport, largely due to an increasing awareness of the harm that contaminated sediment can cause to lake ecosystems and human water use (Chapra, 1997). Our knowledge of the physical processes that control sedimentation has continued to grow as a wider variety of lakes have been studied; still, studies of lake sediment transport are conducted on a case-by-case basis, as the complexity of the problem negates the use of a universal formula or method (Mehta, 2014).

The first section of this chapter provides a three-part conceptual overview of the physical processes that dominate sediment transport in Quesnel Lake: rivers bring in sediment, and take out less than they bring in (section 2.1.1); the sediment that stays in the lake either sinks to the bottom (where it may come back up, section 2.1.2); or remains in suspension (to be transported by currents within the lake, section 2.1.3).

The second section is a summary of two studies that described the physical and chemical changes in Quesnel Lake resulting from the 4 August 2014 spill. The first, by Petticrew et al. (2015), gave an account of these changes between 4 August and 2 October 2014. The second, by Hamilton et al. (2020), extended the study period until November 2017.

2.1 Lake sedimentation processes

2.1.1 Rivers

Most lakes eventually become filled with sediment, transformed on geological timescales into meandering river landscapes (Håkanson and Jansson, 1983). An interesting case in point is Kamloops Lake, a deep, intermontane lake located about 200 km to the south of Quesnel Lake in the Thompson River system. Kamloops Lake is expected to be 98% filled with sediment by 5750 CE (Pharo and Carmack, 1979). This inevitable fate makes sense in light of an observation by Carmack et al. (1979) that Thompson River water is three to four times more turbid at the inflow than at the outflow. Sediment is not only less abundant at the outflow, it is also comprised of smaller particles than at the inflow (Pharo and Carmack, 1979). This illustrates the process of selective settling: large particles settle faster than small particles do, so fewer large particles remain in suspension at the outflow. For a given particle size, a fraction of inflowing sediment will escape via an outflowing river, and the remainder will be buried in the lake bottom. In a study of Lake Laitaure in Lapland, Sweden, Axelsson (1967) showed the relationship between particle size and outflowing/deposited fractions for varying river flow. Under widely varying flow rates (25 to 400 m^3/s), 90-100% of inflowing sediment with a diameter of less than 2 μm remained in suspension at the outflow. In contrast, 0-10% of sediment with a diameter of greater than 20 μm remained in suspension.

At an inflow, the density of river water relative to lake water will control where fine sediment goes within a lake. In Kamloops Lake, coarse sediment (sand) settles on the face of the delta at the inflow of the Thompson River during every season; while fine sediment is carried in a plume of river water which enters the lake differently from season to season, depending on the lake's state of thermal stratification (Carmack et al., 1979). If river water is less dense than surface water in the lake, the plume of river water will form an overflow. Otherwise, a plunge point will form where the inertia of the incoming water is met by the buoyancy of lake surface water. The river plume will then either sink to a level of neutral buoyancy and insert itself into the water column as an interflow, or sink all the way to the bottom and become an underflow. In the case of interflows, plume velocity can also affect sediment deposition, as shown by Scheu et al. (2015) in Lake Maggiore, Italy. The

authors described an increased rate of bottom sediment accumulation occurring under patches of turbulence which arose from shear forces exerted by ambient lake water on the interflowing river plume. Turbulent eddies carry fine sediment particles downward (and upward, and sideways) faster than they can settle; in Lake Maggiore, this can lead to as much as a tenfold increase in sediment deposition over settling alone (Scheu et al., 2015). The chaotic, every-directional transport of turbulence is analogous to diffusion, with the net movement of sediment occurring down-gradient (in the direction of decreasing concentration). Because the river plume has a higher concentration of sediment than the water between the interflow and the lake bottom has, the net transport is down.

In Quesnel Lake, three inflows make up most of the hydrological and natural sediment input: the Horsefly River, the Mitchell River, and the Niagara River (also known as Niagra Creek, Figure 1.1). Gilbert and Desloges (2012) showed that since the last ice age, the highest rate of sediment accumulation has occurred on the lake bottom near the inflow of the Horsefly River in the West Arm. At the inflow of the glacier-fed Niagara River in the East Arm, a bifurcating plume forms while the lake is stratified each summer, with one turbid layer transporting sediment along the seasonal thermocline, and another along the lake bottom (Hamilton et al., 2020). The Mitchell River flows into the North Arm; its sediment contribution is small compared to the other two, because of settling in upstream Mitchell Lake.

2.1.2 Bottom dynamics

Settling naturally leads to an accumulation of particles at the lake bottom. Two outcomes are possible for sediment that has reached the bottom: it may remain on the bottom, to be buried under more sediment, or it may be resuspended (Chapra, 1997). Fine sediment burial is rare on slopes inclining more than 4-5% (Håkanson and Jansson, 1983). The sedimentological record of Quesnel Lake backs this out: across-lake acoustic surveys done by Gilbert and Desloges (2012) show nearly no sedimentation on the sloping sides of the lake, and several tens of meters of sediment in flat layers overlying the bottom bedrock. Seiching is one reason for why so little sediment remains on the sloping sides of a lake long enough to be buried. Some of the fastest, most turbulent currents in lakes occur along slopes, especially during upward motion of the thermocline (Chowdhury et al.,

2016; Marti and Imberger, 2006). When the shear stress caused by bottom friction exceeds a critical value for a given type of sediment, that sediment is resuspended (Bloesch, 1995). For poorly consolidated fine sediment, critical shear stress can be very low, such that even the comparitively gentle shear exerted by seiche currents along the flat bottom can cause resuspension (Gloor et al., 1994). In this case, sediment concentration is higher toward the lake bottom, and shear-driven turbulence will result in the upward transport of sediment.

Sediment resuspension over a sloping bottom is a different matter. In the second paragraph of Chapter 1, we briefly described how seiche-driven resuspension along slopes and subsequent turbulent mixing can lead to either an intrusion that transports sediment horizontally into the lake's interior, like a riverine interflow; or a turbidity current that takes sediment to the bottom, like a riverine underflow (Marti and Imberger, 2006; Wain and Rehmann, 2010). The main difference between river and resuspension sediment input is that the former is continual, while the latter is episodic (Chapra, 1997). In Aya Hayden Lake, Iowa, USA, seiche-induced mixing along a sloping bottom was shown to cause the horizontal transport of material via radially propogating intrusions (Wain and Rehmann, 2010). The intrusions observed in Aya Hayden Lake had a propogation speed on the order of 1 cm/s based on arrival times between CTD stations. Seiche amplitudes of $\sim$0.5 m were associated with this transport, in a basin much smaller than those of Quesnel Lake, where amplitudes of tens of meters are common in the autumn.

2.1.3 Currents between basins

Sediment will remain suspended so long as water movements within the lake carry it upward more than it settles downward. But while settling is decidedly downward, water movements are three dimensional, which can greatly affect the spatial distribution of sediment in a lake. A general discussion of lake dynamics as they relate to sediment transport is beyond the scope of this chapter; for readers wanting to familiarize themselves with the topic, many good introductions have been written on mixing and transport in seasonally stratified lakes (cf. Fischer et al., 1979; Chapra, 1997; Wetzel, 2001c).

There is a particular type of current that is not covered in any introductory texts that we are aware

of; that occurs between basins of lakes with multiple basins (like Quesnel Lake), as well as between oceanic basins (e.g. a fjord connected to the ocean by a shallow constriction); and that plays a central, dynamic role in Quesnel Lake following periods of sustained wind forcing when the lake is thermally stratified. This phenomenon, called seiche pumping, was found by Lawrence et al. (1997) to significantly increase the exchange of oxygen between the north and south basins of Amisk Lake, Alberta. Seiche pumping is the net result of oscillatory, layered flows that exchange water between basins; each cycle is accompanied by some mixing, which over time tends to move suspended and dissolved matter from areas of higher concentration to areas of lower concentration. Gilbert and Desloges (2012) have hypothesized that Quesnel Lake's lowest rate of sediment deposition occurs in the West Basin (0.22 mm annually) not only because the latter lacks major inflows, but also because its hypolimnetic water is flushed by internal seiching (Laval et al., 2008).

What is missing from the observational science of lake sedimentation is a description of what happens to a lot of sediment that is introduced all at once, as can happen in a landslide, a flood, or a tailings dam failure. To that end, our aim is to evaluate the short and long term sedimentary effects of the Mount Polley spill in Quesnel Lake using a mass balance (Chapter 3). Our approach is two-pronged: data and an analytical model, presented in Chapters 4 and 5, respectively.

2.2 Prior accounts of the Mount Polley spill

Most of the sediment that entered Quesnel Lake during the Mount Polley spill settled rapidly to the bottom of the West Basin, as we mentioned in Chapter 1, while a comparatively small fraction remained in suspension. During the spill, the mixture of mine process water, tailings, and eroded surficial material from Hazeltine Creek (together called *slurry*) sank as it entered the warm, clear surface water and then dispersed laterally throughout the deep, cold water of the lower layer, called the *hypolimnion*. Although warm, the slurry was laden with suspended and dissolved material and so was more dense than the lake's water. Through late summer and early autumn 2014 in the West Basin, nearly all of the suspended sediment mass was confined below 30 m depth in a highly turbid, hypolimnetic plume ($>$ 100 nephelometric turbidity units, NTU). The addition of slurry increased hypolimnetic water temperature by ~2.5°C; overlying this 7.5°C hypolimnetic water was a layer

of colder (5°C) water with lower turbidity (~10 NTU). Because fresh water is most dense at very slightly less than 4°C, for 5°C water to be on floating on top of 7.5°C water, dissolved or suspended matter must be present in the lower water mass to increase its density. Petticrew et al. (2015) used this fact to estimate that a minimum of ~30 Gg of sediment was needed to maintain stable stratification in the West Basin through September 2014. Sediments sampled from the hypolimnetic plume during this time exceeded provincial freshwater sediment quality guidelines for total arsenic, copper, iron, and manganese (Golder Associates Ltd., 2015; Petticrew et al., 2015).

Petticrew et al. (2015) reported on three paths through which suspended sediment exited the hypolimnetic plume in the West Basin. On 20 August 2014, the authors showed turbidity exceeding 1000 NTU near the bottom of the West Basin. By 10 September 2014 (the start of our study), turbidity at the same location and depth was around 200 NTU. This decrease was mainly the result of the first path: sediment settling out of suspension and depositing on the bottom. The second path was the Quesnel River, in which the authors observed periods of cool temperature combined with elevated turbidity which they attributed to upwelling in the lake. During upwelling, internal seiche displaces hypolimnetic water to the surface; this tends to occur at the far ends of long, narrow lakes, as is the case with the northern reach of the West Basin where Quesnel Lake flows into the Quesnel River. Upwelling after the spill raised turbid, 7.5°C hypolimnetic water to the surface where it could be drawn into the river. The third path by which suspended sediment left the West Basin, over the Cariboo Island sill, was detected as a layer of turbid water spreading eastward into the main basin of Quesnel Lake, a direction opposed to that of the mean hydraulic flow. The authors suggested this upstream transport could have been due to episodic, seiche-driven flushing of hypolimnetic water. In Chapter 4, we provide evidence of another mechanism for the observed upstream transport: that of a horizontally propagating intrusion, similar to the river interflows that we have discussed above.

2.3 Objectives

One objective of our study is to evaluate the relative importance of the three paths (also called *sinks*) identified by Petticrew et al. (2015) for sediment to leave the West Basin (settling to the bottom, flowing out the Quesnel River, or moving east into the main basin of Quesnel Lake). Another

objective is to evaluate sources of sediment to the West Basin. A follow-up study to Petticrew et al. (2015), authored by Hamilton et al. (2020), has shown seasonal sediment loading to be an ongoing issue for the West Basin. Each autumn of 2015 to 2017, Hamilton et al. (2020) observed a slight turbidity increase (1 to 2.5 NTU) in the West Basin hypolimnion. The authors attribute this yearly increase to bottom currents, driven by seiche, which remobilize an unconsolidated bottom sediment layer. In Chapter 4, we show further evidence that seiching leads to sediment loading each autumn.

Chapter 3

Methods

3.1 Field data collection

In the wake of the August 2014 spill, several organizations either initiated or increased water quality monitoring in Quesnel Lake and the Quesnel River. This study used data collected by provincial and federal government, industry, and public research institutions; the authors are affiliated with a collaboration that we herein refer to as the Environmental Damages Fund (EDF), named for the group which provided financial support through Environment and Climate Change Canada (ECCC).

EDF data include vertical profiles collected in Quesnel Lake using two Seabird Electronics conductivity, temperature, depth (CTD) profilers, both equipped with Seapoint Turbidity Sensors. CTD data from each downcast were depth averaged into 1 m bins. Our West Basin pre-spill CTD dataset consisted of 16 profiles from 12 dates between 2006 and 2012, with data from spring through early autumn, and no data from late autumn or winter. From 10 September 2014 onwards, the 10 CTD stations shown in Figure 1.1 were profiled on a bi-weekly basis during the late April to early December field seasons (71 transects collected during this study period). The pre-spill data and the early years (2014-2017) of post-spill data were collected using an SBE19plus we refer to as the DFO CTD (SN 4057). The 2018 CTD data were collected using the UBC CTD (SBE19plusV2, SN 7035). Turbidity (Tu, formazin turbidity units, FTU) data from each CTD have been corrected to formazin standard.

Continuous, in-lake suspended sediment concentration data came from four moored turbidity sensors (JFE Avanatech Co., model ACLW-USB) and a moored acoustic Doppler current profiler (ADCP; Teledyne RD Instruments, 1200 kHz WH-ADCP). Between November 2014 and October 2018, we deployed three turbidity sensors in the West Basin (4 m and 38 m depth at mooring M3, 10 m depth at mooring ADCP1) and a fourth just east of the Cariboo Island sill (10 m depth at mooring ADCP2, Figure 1.1). Especially with shallower sensors during the warm, late summer and early fall periods, raw turbidity data were often noisy or spiky, indicative of biological fouling (Figure 3.1a). For unknown reasons, negative turbidity values were sometimes recorded; these were removed in the first step of data processing. In the second step, we removed those periods of each turbidity time series for which standard deviation calculated over a 6 hour sliding window (25 samples) exceeded 12%. We chose a 6 hour interval to allow for diurnal fluctuation and found, through trial and error, that a standard deviation threshold of 12% was effective for removing large, random spikes. In the third step, we corrected each time series for sensor drift, which may have been the result of mechanical wearing on the sensor by the wiper, leading to gradually increasing turbidity. As an example, during the third deployment period (2 October 2015 to 27 September 2016), SBE turbidity data from both 4 and 38 m at station ST9 (Figure 1.1) showed a decreasing, overall trend, while JFE data from these depths on mooring M3, especially the 38 m sensor, showed an increasing trend (Figure 3.1a). For each turbidity time series, we matched the trend of the JFE data to that of the SBE data by rotating the former to conform to the slope of the latter. Figure 3.1b shows JFE turbidity data which have been corrected for drift (and, prior to that, noise), along with the turbidity values used for the fourth and final step: determining a scale and offset for correction to formazin standard. Here we computed the slope and offset for each JFE turbidity time series using linear, least squares regression of JFE to SBE turbidity data (Figure 3.1c).

Echo intensity recorded by the downward-facing, 1200 kHz ADCP on mooring TuADCP served as a proxy for turbidity, based on the relation:

$$Tu_{(est)} = 10^{A*R_B+B}, \tag{3.1}$$

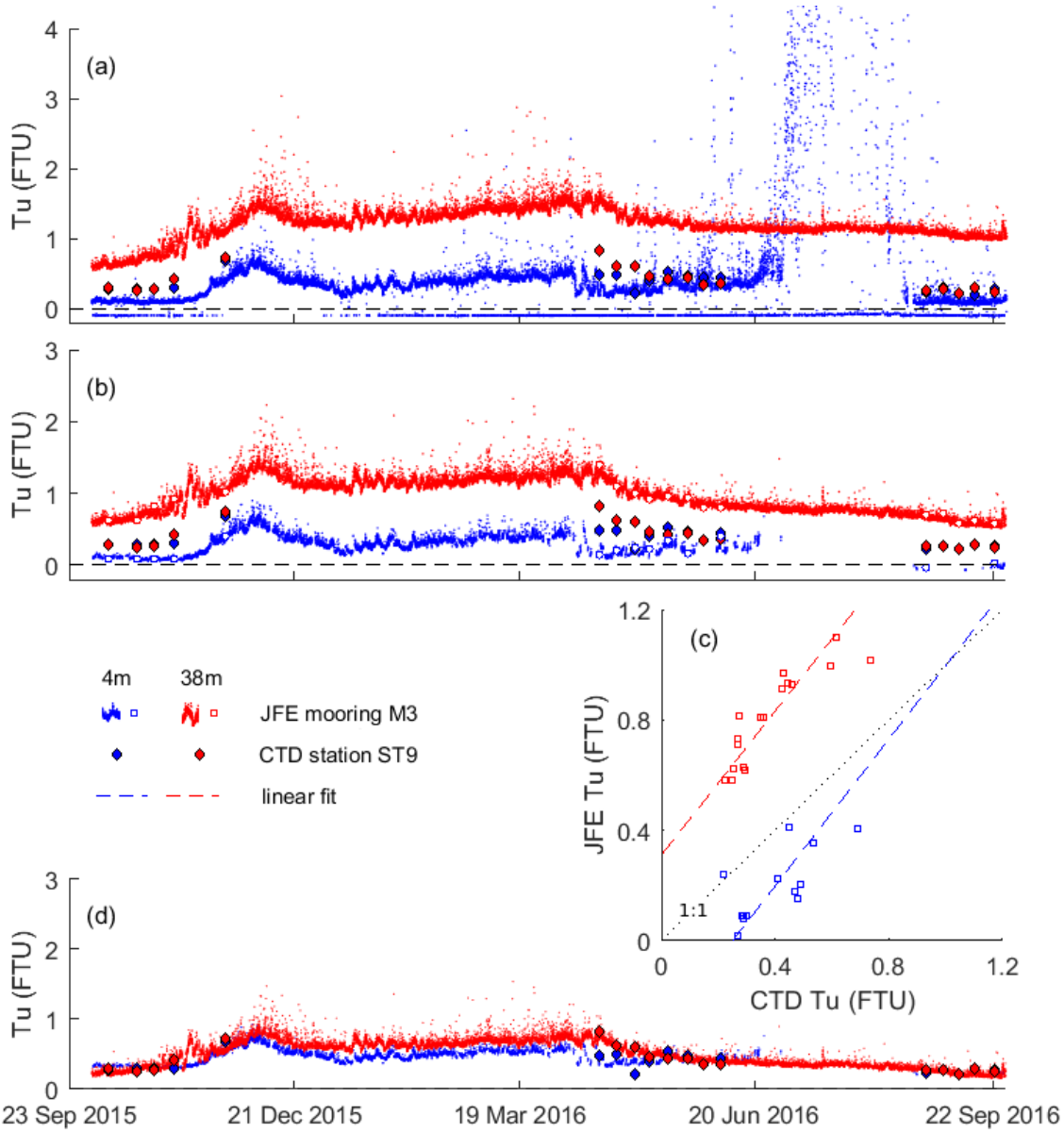

Figure 3.1: Moored (JFE) sensor turbidity data processing. Two example time series are depicted from the 23 September 2015 to 22 September 2016 deployment period. Raw turbidity is shown in (a); spikes and drift were removed to give the turbidity data shown in (b). Panel (c) shows the JFE and SBE (CTD) turbidity data that we used to determine slope and offset; with the resulting formazin-standardized turbidity time series appearing in (d).

where R_B is relative backscatter, in decibels (dB), and A and B are constants determined by linear regression to CTD turbidity measured at station ST10. Following Gartner (2004), we calculated R_B by converting echo intensity (E, counts) to echo power (decibels, dB) and adding losses for beam spreading and sound absorption, as:

$$R_B = k_E(E - E_r) + 2\alpha R + 20log_{10}R, \tag{3.2}$$

where α is the sound absorption coefficient (dB/m) for water (we used the formula of Francois and Garrison, 1982); R is the distance (m) along the beam to the depth bin being measured; E_r is the system noise floor, taken as the lowest recorded E for each of the four transducer beams; and k_E is a beam-specific calibration constant. For a 1200 kHz RDI ADCP, k_E ranges from 0.35 to 0.55 dB/count (Deines, 1999). In his San Francisco Bay study, Gartner (2004) had neither manufacturer-supplied nor laboratory-calibrated k_E values, and lacking these or physically-based alternatives, used $k_E = 0.45$ dB/count. Like Gartner, we did not have predetermined k_E values for our ADCP. But unlike San Francisco Bay, suspended sediment concentration in Quesnel Lake was rarely above 1 g/m^3 during the ADCP's deployment (Chapter 4), and an accurate k_E was needed to resolve turbidity through depth in these low-sediment conditions. During servicing and redeployment on 3-4 October 2017, the ADCP was repositioned from 8 m to 12 m above bottom. This allowed us to compare time series of R_B from the first deployment to corresponding depths from the second. We averaged the four echo powers of each 0.5 m bin before adding losses from spreading and absorption to get R_B from equation (3.2) (Figure 3.2a). The multicolored line in Figure 3.2a represents four echo power time series ($k_E(E - E_r)$), one from each transducer, from the 0.5 m bin closest to 102 m depth, or 6 m above bottom. During the first deployment (30 September 2016 to 3 October 2017), this was the fourth bin; and during the second (4 October 2017 to 26 September 2018), the twelfth. Starting at 0.45 dB/count, we adjusted k_E iteratively until R_B was aligned between deployments for bins at 102, 104, and 106 m depth, and in this way arrived at $k_E = 0.37$ dB/count. A time series of ADCP echo-based turbidity estimates at these three depths is given in Figure 3.2c, along with the linear regression of R_B to Tu measured at CTD station ST10 (Figure 3.2b) that was used to

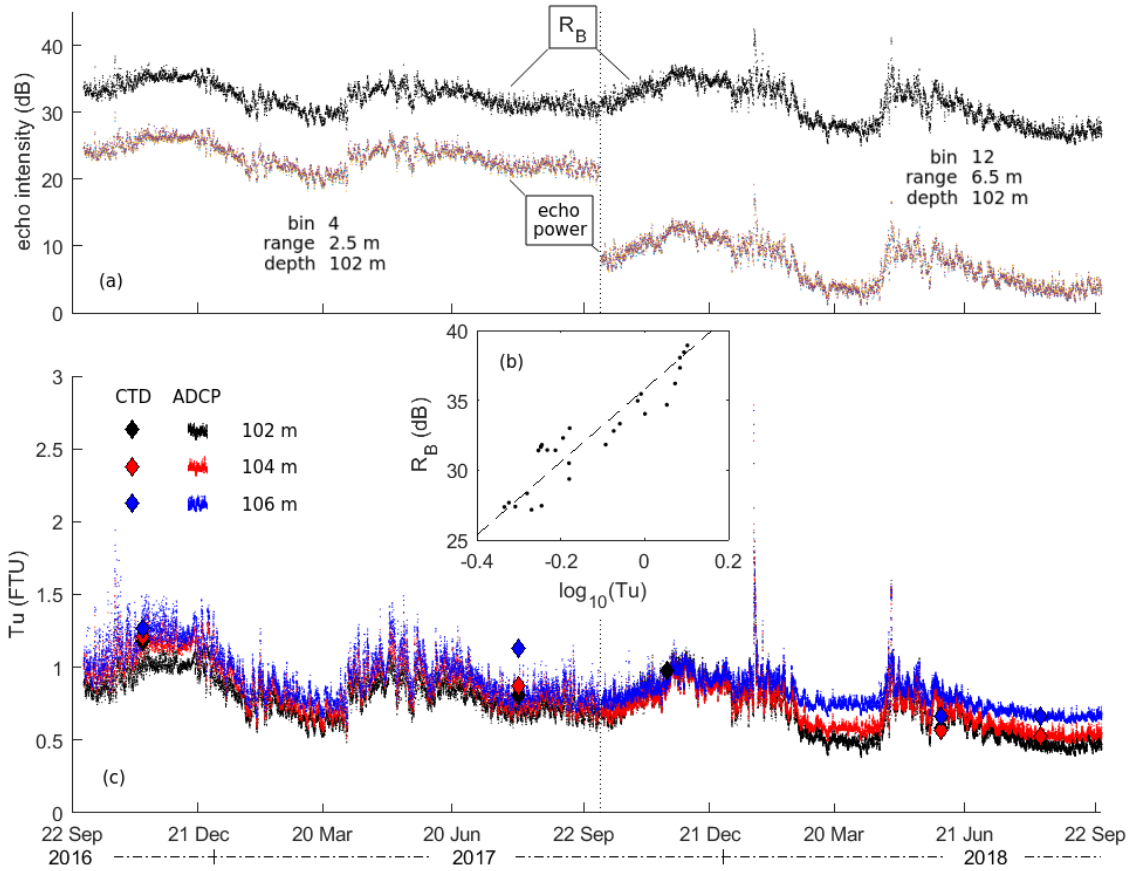

Figure 3.2: Turbidity estimates from ADCP echo. The multicolored lines in (a) represent echo power (four beams) in the bin corresponding to a depth of 102 m; after averaging the four echo powers, losses from beam spreading and sound absorption have been added to give relative backscatter (R_B, dB). In (b), the dotted line indicates best fit from the log-linear regression of R_B to CTD turbidity (Tu, FTU) measured at station ST10; the the dotted line's slope and offset correspond to the constants A and B, respectively, in equation (3.1). The resulting echo-based turbidity time series estimates are shown for three depths in (c).

determine the constants A and B used in equation (3.1).

In addition to its two turbidity sensors, mooring M3 had 15 thermistors (RBR duoTD, duoCT, and soloT; depths: 4, 8, 13, 18, 23, 28, 33, 38, 43, 53, 63, 73, 78, 83, 93, and 103 m). In section 4, we have used their temperature data along with velocity data from the 1200 kHz ADCP at mooring TuADCP to show how thermal stratification and internal wave-driven currents relate to sediment transport.

Through the first winter post-spill, Mount Polley Mining Corporation (MPMC) used a CTD

profiler (YSI EXO2 Sonde) to measure physical data in Quesnel Lake. As far as we are aware, these profiles were the only high vertical resolution turbidity data collected during this period. Herein we include turbidity data from 14 profiles collected between 1 November 2014 and 30 May 2015; these compare well to EDF turbidity profiles (DFO CTD, formazin-standardized values) taken within a few days from the nearest station (ST9, Figure 1.1) in November 2014 and May 2015.

ECCC monitors turbidity in the Quesnel River through the Federal-Provincial Freshwater Quality Monitoring and Surveillance Network (FWQMS), and flow (Q, m^3/s) through the Water Survey of Canada. We used these data to estimate suspended sediment concentration and mass flow in the Quesnel River (described in section 3.3). We have assumed the river to be completely mixed, such that a point sample of turbidity collected at mid-span from Likely Bridge (Figure 1.1) is representative of the cross section. In the year following the spill, sampling occurred weekly, and then bi-weekly or monthly thereafter. Between sample dates, we estimated turbidity by linear interpolation. For comparison, we have also included continuous in-river turbidity measurements made by MPMC at a location 1.5 km downstream of Likely Bridge (MPMC, 2015), as well as in-lake turbidity near the outflow recorded by a moored EDF sensor (10 m depth on mooring ADCP1) and the EDF CTDs (3 m depth at station ST11, Figure 1.1).

3.2 Mass concentration from turbidity

Herein we have estimated suspended sediment mass concentration ($c \equiv m/V$, where m is mass and V is volume) from turbidity. The relationship of turbidity to mass concentration varies greatly for different sediment types, so we developed a site-specific correlation in the laboratory. Using linear, least-squares regression, we calculated slope (k_c) and offset ($Tu_\emptyset$):

$$c = k_c Tu + Tu_\emptyset, \tag{3.3}$$

for a suspension of a given particle size distribution. The sediment we used was collected as a core sample, using a slocore device, from the deep part of the West Basin offshore of Hazeltine Creek on 17 June 2016 (Hatam et al., 2019). The core's uppermost sediment had been removed by an

earlier experiment, and our dry sample had a coarser size distribution ($D_{50} \approx 10\mu$m) than Petticrew et al. (2015) found below 35 m depth, six weeks post spill ($D_{50} \approx 1\mu$m). By mass, large particles contribute less to turbidity than do finer particles, making the correlation of c to Tu sensitive to the particle size distribution of the suspension. To remove large particles, we mixed sample sediment into distilled water in a 70 cm high, 10 cm diameter tube and left the suspension to settle for periods varying from one day to two weeks (Table 3.1). We then used a 2 mm diameter hose to siphon off the supernatant suspension. In this way we obtained four suspensions of varying median particle diameter with which we developed $c(Tu)$ correlations through laboratory tests.

We determined the c of each suspension by filtering 100 mL (suspensions A, B, and C) or 250 mL (suspension D) through 0.45 μm pore diameter papers (in triplicate) and weighing the dry mass of sediment retained. Over four trials (one for each suspension), we immersed the CTD turbidity sensors in a continually stirred bucket of distilled water ($V = 6$ L), covering the bucket to limit ambient light interference as we ran each CTD (i.e., DFO and UBC) in turn for 1 minute. We then uncovered the bucket, measured turbidity using a benchtop turbidimeter (Hach), and added an increment (10 or 20 mL pipette) of suspension, repeating until turbidity reached 7 FTU (typically 10 increments). This turbidity is roughly double the highest recorded in situ between 2015 and 2017 (Hamilton et al., 2020). The benchtop turbidimeter served as our reference instrument, as we calibrated it to formazin standard during each trial (two point calibration at $<$0.1 and 20 FTU). For both the dry sample and the finer suspensions, we measured effective particle size distribution (no pre-treatment) with a laser particle size analyser (Malvern Mastersizer Hydro 2000).

We found the $c(Tu)$ correlation in the 0 to 7 FTU range to be effectively linear for each of the twelve combinations we tested (three instruments with four suspensions). Offset ($Tu_\emptyset$, distilled water turbidity) varied most for the DFO CTD (minimum: 0.52 FTU, maximum: 0.93 FTU, Figure 3.3a), less for the UBC CTD (0.22 to 0.25 FTU), and least for the benchtop turbidimeter (0.10 to 0.11 FTU, Figure 3.3b). Slope (k_c, sensor response) was lowest for the DFO CTD (0.50 to 0.62 g/m^3/FTU, not shown), slightly higher for the UBC CTD (0.54 to 0.68 g/m^3/FTU, not shown), and highest for the benchtop turbidimeter (0.66 to 0.93 g/m^3/FTU, Figure 3.3b).

To assess CTD offset ($Tu_\emptyset$), we looked to data collected during the latter half of our study at

Table 3.1: Four suspensions used in laboratory testing: settling time (t_{settle}); median particle diameter (d_{50}); mass concentration (c, 0.45 μm filter); and turbidity (Tu). Note that suspension D was too dilute to be measured by the particle size analyser.

suspension	A	B	C	D
t_{settle} (h)	21.5	43	72	307
d_{50} (μm)	5.8	2.1	1.6	-
c (g/m^3)	114 ± 1	165 ± 2	142 ± 9	54 ± 3
Tu (FTU)	184 ± 4	319 ± 6	257 ± 5	90 ± 2

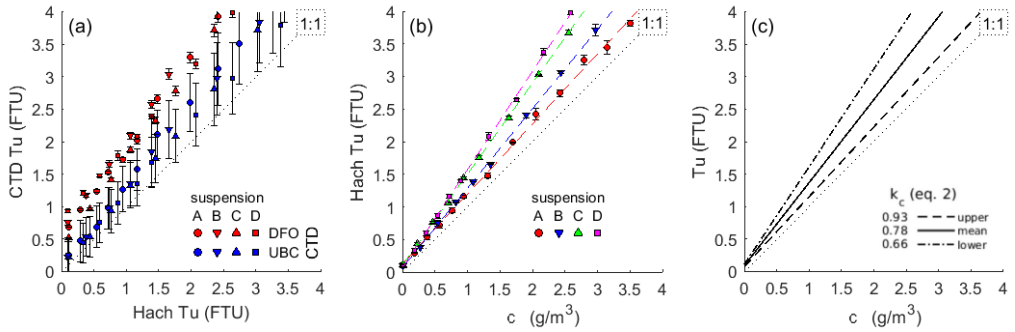

Figure 3.3: c-Tu laboratory results: (a) Seapoint (two CTDs, y-axis) compared to benchtop (Hach, x-axis) Tu (FTU), the latter calibrated to formazin standard. Markers with errorbars indicate the mean and one standard deviation of CTD data from each dilution ($\approx$ 240 samples). (b) Hach turbidity for varying c, with errorbars indicating one standard deviaton (3 samples). Dashed lines show linear fit (least-squares regression) of each suspension's c-Tu correlation (Pearson's $r \geq 0.99$). (c) upper, expected, and lower values of k_c that we use in equation (3.3).

the station furthest from the West Basin (ST8, Figure 1.1). Here, the lowest turbidities measured were 0.14 FTU for the DFO CTD, and 0.10 FTU for the UBC CTD, both in the range of $Tu_\emptyset$ for the benchtop turbidimeter. The $Tu_\emptyset$ variation seen with the CTDs in the laboratory could have resulted from sensor interference (ambient light and/or reflections of the incident beam off the bottom/sides of the bucket and the water surface). The design of the benchtop turbidimeter limits interference, and CTD turbidity data collected at station ST8 indicated that interference is also limited in situ. Herein we scale CTD turbidity to the benchtop reference, using the average ratio of CTD k_c to benchtop k_c from four suspension trials (0.7 for the DFO CTD and 0.75 for the UBC CTD). We take distilled water turbidity to be $Tu_\emptyset = 0.1$ FTU.

The nominal accuracy of a Seapoint Turbidity sensor is $\pm$ 2% of measured values (Seapoint, 2013). Figure 3.3 (a) shows standard deviations of the UBC CTD that are greater than we would expect for a nominal accuracy of 2%, while DFO CTD standard deviations are within the expected range. We swapped the two sensors in the laboratory and found that random fluctuations in the UBC CTD turbidity data were originating in the sensor. As mentioned, we depth average CTD turbidity into 1 m bins. A nominal profiling velocity of 1 m/s (actual profiling velocity is typically slightly less) and a 4 Hz sample rate gives four samples per bin. Averaging CTD laboratory data into four sample bins caused standard deviation to decrease slightly for the DFO CTD, and by about half for the UBC CTD. For upper and lower bound c estimates in Quesnel Lake, we have included an instrument error of $\pm$ 2% for the DFO CTD, and $\pm$ 10% for the UBC CTD.

Australian Laboratory Services (ALS) processed the FWQMS water samples collected from the Quesnel River. For these turbidity data, we have assumed the ALS turbidimeter performs similarily to our benchtop (Hach) unit. Such instruments have a nominal accuracy of $\pm$ 2%. In our laboratory tests, the standard deviation from three measurements of a given sample was typically between 1 and 3% of the mean. For upper and lower bound c estimates in the Quesnel River, we have used an instrument error of $\pm$ 6% (two standard deviations about the mean).

3.3 Conceptual model

Conservation of mass gives that, provided suspended sediment m does not undergo chemical transformation over the time scale of interest, its rate of change in a basin is equal to the sum of mass flows across the basin's boundaries ($dm/dt = \Sigma\dot{m}$). For the West Basin, we have considered mass flows associated with four boundaries: to the north, the Quesnel River ($\dot{m}_r$); along the bottom ($\dot{m}_b$); the shoreline (i.e. inflowing streams, $\dot{m}_s$); and to the east, the main basin of Quesnel Lake ($\dot{m}_l$). For the river, $\dot{m}_r$ is always negative, while for stream inflows, $\dot{m}_s$ is always positive. The sign of $\dot{m}_b$ depends on whether settling ($\dot{m}_b < 0$) or resuspension ($\dot{m}_b > 0$) dominates; and the sign of $\dot{m}_l$ depends on whether the net flow of sediment mass over the Cariboo Island sill is eastward ($\dot{m}_l < 0$) or westward ($\dot{m}_l > 0$).

We calculated upper and lower bounds of West Basin suspended sediment m from vertical tur-

bidity profiles collected at five CTD stations (ST6, ST7, ST9, ST10, and ST11, Figure 1.1) as follows: from each set of five profiles, make an upper bound vertical Tu profile comprised of the maximum observed values across all profiles for each 1 m depth bin, and likewise use minimum Tu to make a lower bound vertical profile; add/subtract sensor error to upper/lower bound Tu profiles; convert these to vertical c profiles using equation (3.3) with upper/lower k_c estimates; and integrate each through the West Basin's volume-depth curve ($V(z)$, z positive downwards, $z_b = 108$ m):

$$m = \int_0^{z_b} c(z)V(z)dz. \tag{3.4}$$

Our best estimate (expected m value) is based on the median turbidity across all profiles for each bin, with $c(z)$ from equation (3.3) using the average k_c of the four suspensions given in Table 3.1, and the same $V(z)$ curve as we use for upper and lower m bounds.

For the Quesnel River, we used daily-average flow (Q) to estimate sediment mass flow ($\dot{m}_r$, Mg/day) as:

$$\dot{m}_r = Q \cdot c \cdot 0.0864 \frac{\mathrm{s \cdot Mg}}{\mathrm{day \cdot g}}, \tag{3.5}$$

with upper bound, expected, and lower bound c from equation (3.3) using FWQMS turbidity data. We estimated turbidity between bottle sample dates by linear interpolation. Section 4 gives cumulative mass flow (Mg) by solar season, which we calculate by multiplying $\dot{m}_r$ from equation (3.5) by $\Delta t = 1$ day and summing over the number of days between equinox and solstice. Throughout the text, the terms *summer, autumn, winter,* and *spring* correspond to the solar year, except when followed by a state of stratification (e.g. *spring mixis* or *winter inverse stratification*).

Suspended sediment collected in bottle samples from 30, 60, and 90 m depth in the West Basin on 18 September 2014 had a median particle diameter slightly smaller than 1 μm (Petticrew et al., 2015). For a particle with a diameter $d = 10^{-6}$ m and density $\rho_p = 2500$ kg/m^3, the Stokes' settling velocity (w_s, m/s) is:

$$w_s = \frac{g}{18} \frac{(\rho_p - \rho_f)}{\mu} d^2 = 5.6 \cdot 10^{-7} \mathrm{m/s} \approx 5\,\mathrm{cm/day}. \tag{3.6}$$

where $g = 9.8$ m/s^2 is the gravitational constant, $\rho_f = 1000$ kg/m^3 is fluid density, and $\mu = 0.0015$ kg/ms is the dynamic viscosity of the fluid (cf. Håkanson and Jansson, 1983, Chapter 6). Using this velocity, we calculated an approximate settling mass flow rate ($\dot{m}_b$) for the date of each West Basin $c(z)$ profile as:

$$\dot{m}_b = -\int_0^{z_b} c(z) w_s A(z) dz, \tag{3.7}$$

where $A(z)$ is the bottom area at depth z. For dates between $c(z)$ profiles, we estimated $\dot{m}_b$ using logarithmic interpolation; i.e., linearly interpolating $ln(\dot{m}_b)$. We do not give upper and lower bounds for $\dot{m}_b$; rather, we treat these as order-of-magnitude estimates, reflecting their uncertainty (the exact conditions affecting settling are complex, as the vertical velocity component of currents may enhance or negate a particle's downward motion through the water; cf. Gloor et al., 1994; Scheu et al., 2015).

Chapter 4

Results

Prior to the 4 August 2014 spill, turbidity in the West Basin was typically low (< 0.4 FTU), with some instances of higher turbidity near the surface during spring (Hamilton et al., 2020). Since our $c(Tu)$ correlations are based on sediment from the spill, they may not be accurate for natural sediment. Still, we need a point of reference to be able to say what normal sedimentary conditions are in Quesnel Lake. Lacking a better alternative with which to estimate pre-spill c from turbidity (such as a bulk sample of natural sediment to use in laboratory calibrations), we apply equation (3.3) with the same linear coefficients used for post-spill turbidity data (Figure 3.3). Doing so, we find a maximum $c \approx 1.1$ g/m^3 observed between 1 and 3 m depth in the West Basin on 3 June 2008 (Figure 4.1a); this would have most likely been associated with a riverine overflow. Hypolimnetic sediment c in the West basin was typically < 0.2 g/m^3. Using the median and maximum c observed in the pre-spill data at each depth in the West Basin, based on equation (3.4), the approximate pre-spill median and maximum m were 75 and 280 Mg, respectively (Table 4.1). Note: from here on, to avoid switching between metric prefixes, we will describe mass in units of Mg (1 Mg $=$ 1000 kg $=$ 1 ton).

Quesnel Lake's response to the Mount Polley spill has unfolded in two phases (Hamilton et al., 2020). Here we mark the end of the first phase (referred to as the *initial regime*, section 4.1) as the approximate date when the total mass of sediment in the West Basin first fell below the historical maximum value; as we shall see, this occurred around early June 2015, ten months following the

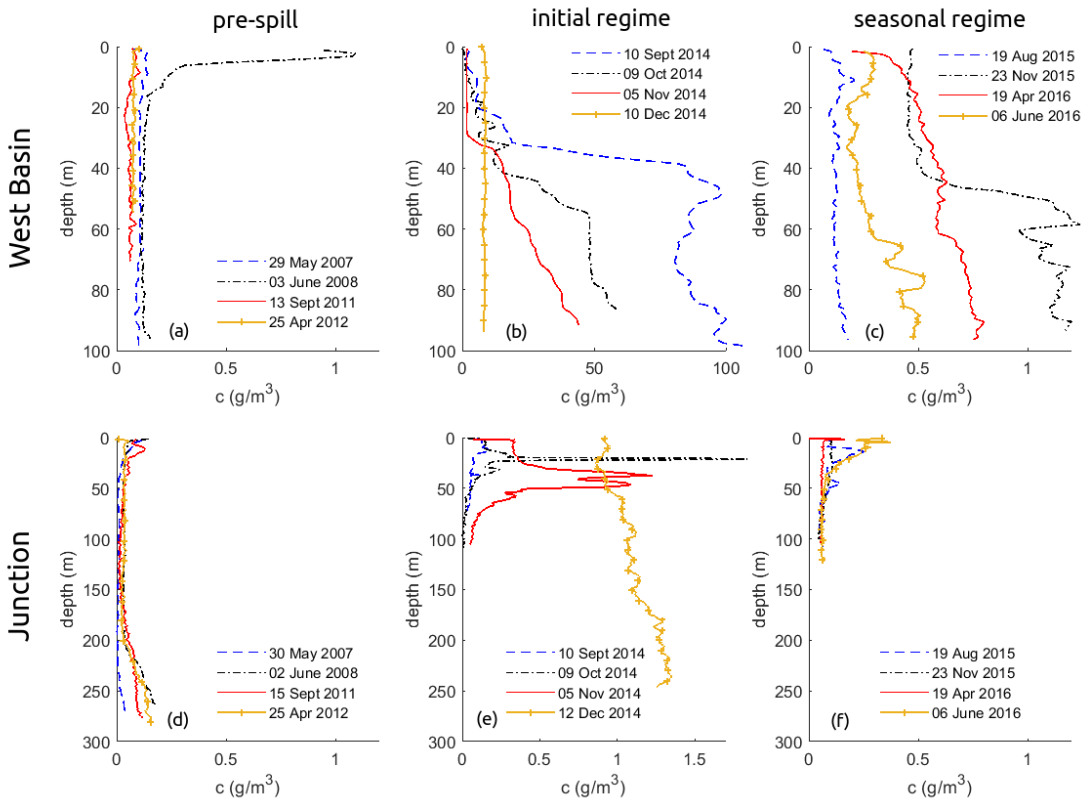

Figure 4.1: Vertical profiles of suspended sediment concentration at CTD station ST9 in the West Basin (a-c) and ST8 near the Junction (d-f). Note the change in scale for the x-axes of (b) and (e), and the differing y-axes for the West Basin and the Junction.

spill. The subsequent, seasonal regime (section 4.2) appears to be ongoing; we will use the pre-spill median suspended sediment *m* in Chapter 5 as a benchmark to define when the seasonal regime will have ended (i.e., how long Quesnel Lake will take to recover from the sedimentary effects of the spill.)

4.1 Initial regime

Let's return to the ∼30000 Mg of suspended sediment that Petticrew et al. (2015) estimated to be in suspension below 30 m depth in the West Basin hypolimnion in early summer/late autumn 2014, based on water column stability (described in section 2.2). On 10 September 2014, West Basin hypolimnion concentrations measured at CTD station ST9 ranged from 20 g/m^3 at 30 m depth to over 100 g/m^3 near the bottom (Figure 4.2a). Applying equation (3.4) to the 10 Sept 2014,

Table 4.1: Suspended sediment mass in the West Basin by date. Error estimates are only given for mass based on EDF CTD data, as transects capture spatial variation in suspended sediment concentration. Mass data are also presented in Figure 4.2b.

date	event	m (Mg)
-	pre-spill median	75
-	pre-spill maximum	280
03 June 2008	CTD cast (Figure 4.1a)	230
04 Aug 2014	Mount Polley spill	-
10 Sept 2014	CTD transect (Figure 4.1b)	38000 ± 11000
22 Sept 2014	autumnal equinox	25000
09 Oct 2014	CTD transect (Figure 4.1b)	17000 ± 5000
05 Nov 2014	CTD transect (Figure 4.1b)	9200 ± 1900
22 Nov 2014	onset of autumnal mixis	7600
10 Dec 2014	CTD cast (Figure 4.1b)	7600
21 Dec 2014	winter solstice	6000
20 Mar 2015	spring equinox	1300
24 Mar 2015	onset of spring mixis	1300
03 June 2015	end of initial regime (approx.)	300 ± 110
21 June 2015	summer solstice	240
26 August 2015	yearly minimum	140 ± 30
23 Nov 2015	seasonal regime maximum	600 ± 140

horizontally averaged West Basin $c(z)$ profile (not shown, but similar to the station ST9 $c(z)$ profile) gives a mass of 38000 ± 11000 (Table 4.1), putting Petticrew et al. (2015)'s stability-based estimate within range of our turbidity-based estimate.

Through autumn 2014, West Basin surface c gradually increased (Figure 4.2), until the initially clear surface water had become visibly green. Hamilton et al. (2020) gave an account of surface mixed layer deepening and entrainment of the turbid, hypolimnetic water that led to this "greening." This surface color change had occurred by mid-November 2014. By 10 December, c was near 7 g/m^3 through depth near CTD station ST9 (Figure 4.1). Temperature data presented in Hamilton et al. (2020) likewise indicate that the West Basin was fully mixed at this time, which is also consistent with sediment c near 7 g/m^3 in the Quesnel River (Figure 4.2d). Based on the $c(z)$ profile shown in Figure 4.1b, approximately 7600 Mg of sediment was suspended in the West Basin on 10 December 2014 (Table 4.1). By 3 June 2015, m had decreased to 300 ± 110, approaching the pre-spill maximum m. Thus, over nine months between 10 September 2014 and 3 June 2015, West Basin suspended sediment m had decreased by two orders of magnitude. With this in mind, we will

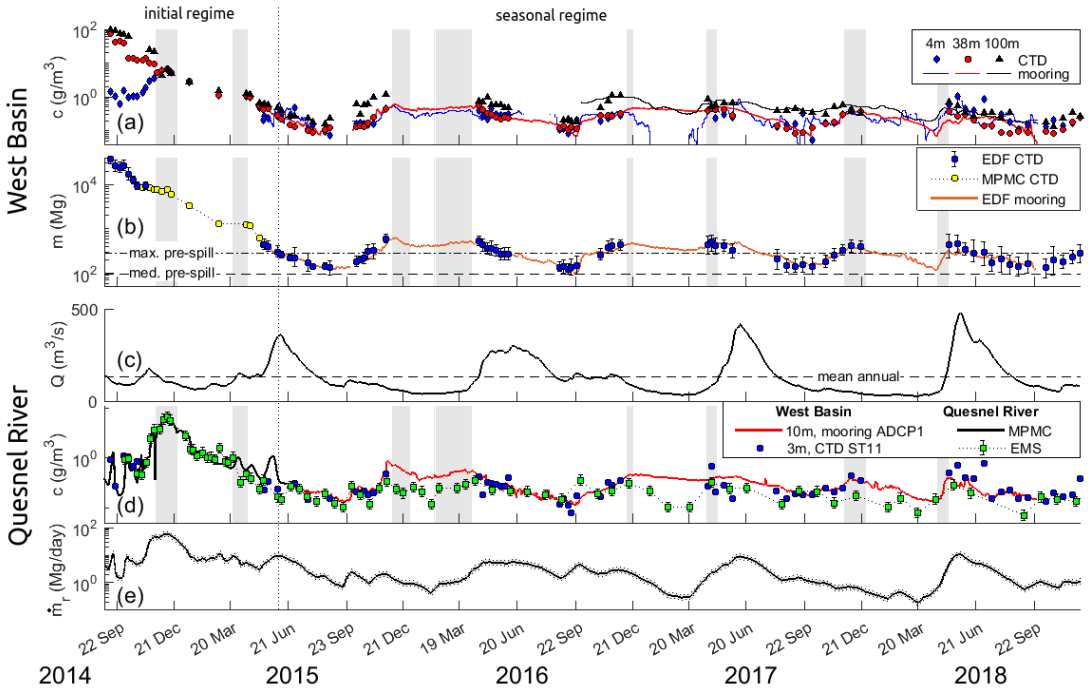

Figure 4.2: Suspended sediment timeline, 10 September 2014 to 21 December 2018: (a) West Basin concentration at three depths (note: 4 and 38 m depth c are based on turbidity, while 95 m depth c is based on acoustic echo intensity (ADCP) data; and, to improve readability, processed JFE data (Figure 3.1d) and ADCP data (Figure 3.2c) are smoothed with a 1 week moving average); (b) West Basin mass (upper and lower bounds given by errorbars); Quesnel River (c) daily averaged flow; (d) concentration; and (e) mass flow (upper and lower bounds given by grey shaded region). In (a), (b), and (d), grey shading indicates periods of mixis.

now turn to the sinks responsible for this decrease in West Basin sediment m: the Quesnel River, settling, and exchange flows.

The Quesnel River had its part in removing sediment during the inital regime, accounting for 4000 ± 1000 Mg, or just over 10% of the total decrease in West Basin m between 10 September 2014 and 3 June 2015 (Table 4.2). Sediment c in the river at the sampling location is controlled by surface c in the West Basin, as that part of the channel has no inflowing tributaries or eroding banks, and until October 2014 the surface mixed layer (epilimnion) had not entrained enough sediment from the hypolimnion to cause an appreciable increase in river mass flow, $\dot{m}_r$, based on equation (3.5). Through October and November, the surface mixed layer deepened in Quesnel Lake, and $\dot{m}_r$ increased as lake surface c increased (Figure 4.2e). On 11 December 2014, with the West Basin in

Table 4.2: Cumulative mass flows by period within the initial regime for each of three West Basin suspended sediment mass sinks: the Quesnel River, equation (3.5) integrated through time; settling, equation (3.7) integrated through time; and exchange with the main basin, estimated from the West Basin's sediment mass balance.

period	Ques. R. (Mg)	settling (Mg)	exchange (Mg)
10-22 Sept 2014	70 ± 15	700	12000
autumn 2014	2200 ± 600	2000	15000
winter 2015	1200 ± 250	250	3200
spring 2015	600 ± 150	80	400
total	4000 ± 1000	3000	31000

autumnal mixis, river c and $\dot{m}_r$ peaked at 7 g/m^3 and 58 ± 14 Mg/day, respectively. The 4000 ± 1000 Mg of sediment that flowed into the Quesnel River during the initial regime represents nearly two-thirds of the cumulative river mass flow observed over our study period (6900 ± 1500 Mg between 10 September 2014 and 21 December 2018).

Similarily, a small fraction of the initial West Basin m decrease can be attributed to settling (Table 4.2). Equation (3.7) states that settling mass flow ($\dot{m}_b$) will decrease as concentration decreases: the West Basin $c(z)$ profile for 10 September 2014 gives $\dot{m}_b = 62$ Mg/day; for 10 December 2014, 8 Mg/day; and for 13 April 2015, 1.4 Mg/day. In total, settling during the initial regime (between 10 September 2014 and 3 June 2015) accounts for about 8% of the decrease in West Basin suspended sediment m for that regime.

Thus, during the initial regime, river outflow and settling combined account for only about 20% of the observed decrease in West Basin sediment mass. The mass balance for the West Basin therefore suggests that most ($\sim$80%) of the sediment mass in suspension on 10 September 2014 flowed east out of the West Basin, over the Cariboo Island sill, and into the main basin of Quesnel Lake (Table 4.2). The elevated c found on 12 December 2014 near the Junction (Figure 4.1e) supports this conclusion. CTD data presented by Petticrew et al. (2015) showed that sediment mass flow east over the sill ($\dot{m}_l$) had begun by early August. They observed a continuous, turbid layer that propagated east along the density interface (i.e. thermocline at $z \approx 20$m). Based on relative arrival times at CTD stations, the authors estimated a propogation speed of $\sim$1 cm/s. By 18 September 2014, this layer had passed CTD station ST0 in the West Arm (Figure 1.1). Four kilometers west at

station ST2, the layer was found between 15 and 40 m depth with c up to 6 g/m^3.

To find an approximate scale of the $\dot{m}_l$ associated with this layer, we first consider the physical mechanism for its propagation. In the Sea of Galilee (also called Lake Kinneret or Tiberius), second-vertical-mode seiche motions have been shown to constrict the metalimnion, forcing its horizontal displacement as a "metalimnetic jet." Horizontal current velocities of 25 cm/s transport suspended material from the periphery to the interior of Lake Kinneret (Marti and Imberger, 2006). Another plausible mechanism for the turbid layer observed in Quesnel Lake is that of a buoyancy-driven horizontal intrusion (Manins, 1976). We assume the intrusion (turbid layer) crosses the lake's full width and is propagating along its long axis, a reasonable assumption considering the West Arm is around 2 km wide and a distance of some 20 km separates station ST2 from Cariboo Island. A laterally bounded intrusion of height h will propagate at $u_p \approx 0.2Nh$, where $N = \sqrt{g\Delta\rho/\rho_0 h}$ is the average buoyancy frequency across the intrusion of height h, with reference density $\rho_0 =$ 1000 kg/m^3 (Scheu et al., 2015). In the case of station ST2 on 18 September 2014, $u_p = 4$ cm/s. Comparing the scales of second-vertical-mode seiche velocity and theoretical intrusion propogation speed, we find the latter to be closer to the observed 1 cm/s. Multiplying this observed velocity by the cross-sectional area of the West Arm between 15 and 40 m depth at station ST2 ($\sim$63000 m^2), and an average c of 3.5 g/m^3, gives $\dot{m}_l \approx 190$ Mg/day, roughly three times that of $\dot{m}_b$ (settling) for mid-September 2014.

We have shown that between 10 September 2014 and 21 December 2018, suspended sediment m in the West Basin underwent a two order of magnitude decrease, which the mass balance attributes mainly to sediment carried into the main basin of Quesnel Lake by exchange flows. We gave an estimated scale for eastward mass flow for 18 Sept 2014, but our limited information did not allow us to integrate eastward mass flow through time as we do for mass flow in the Quesnel River. Nonetheless, we were able to infer the cumulative mass flow associated with eastward mass flux for a given period using a mass balance for the West Basin.

4.2 Seasonal regime

Suspended sediment m in the West Basin continued decreasing through summer 2015, the first summer of the seasonal regime (Figure 4.2b), eventually reaching a minimum of 140 ± 30 Mg (Table 4.1). On 19 August 2015, the $c(z)$ profile measured at CTD station ST9 showed West Basin c in the range of pre-spill levels through depth (Figure 4.1c). As was the case for the initial regime, this decline in West Basin sediment c and m over the first summer of the seasonal regime was due to sediment being flushed either down the Quesnel River or into the main basin of Quesnel Lake, or, to a lesser extent, settling to the bottom of the West Basin (settling mass flow was $\dot{m}_b \approx 1.4$ Mg/day on 13 April 2015, compared to river $\dot{m}_r \approx 5$ Mg/day). But whereas suspended sediment m only decreased during the initial regime, m underwent periods of increase during the seasonal regime, most notably through the breakdown of stratification each year as the lake approached autumnal mixis (Figure 4.2b). Later in this section, we will describe the conditions associated with increasing suspended sediment m in the West Basin.

But first: an overview of the West Basin's seasonal suspended sediment cycle (first described by Hamilton et al., 2020), for which we shall use the year 2016 as our central example (mainly because this was the first autumn period for which we have bottom velocity data from mooring TuADCP; Figure 1.1). At the onset of stratification in April, c increased slightly through depth (Figure 4.1c), and also increased westward toward the outflow (Figure 4.3b). Summer stratification was always the longest period of a given yearly cycle (Figure 4.2), leading to the lowest overall suspended sediment c in the West Basin. Through spring into summer, c decreased first in the upper water column (Figure 4.3c), and by September approached yearly minimum levels through all depths (Figure 4.3d).

Part way through the autumn breakdown of stratification, on 11 November 2016, a marked c increase appeared in the lower half of the West Basin water column (Figure 4.3e; Figure 4.4d; Figure 4.5a-c), similar to the previous year, where elevated c was found below 40 m depth at CTD station ST9 on 23 November 2015 (Figure 4.1c). Upper water column c increased as the lake approached autumnal mixis in 2016, with c slightly lower in the surface mixed layer (4 m and 38 m depth) than c measured at the bottom (100 m depth, Figure 4.2a). Surface mixed layer c stopped

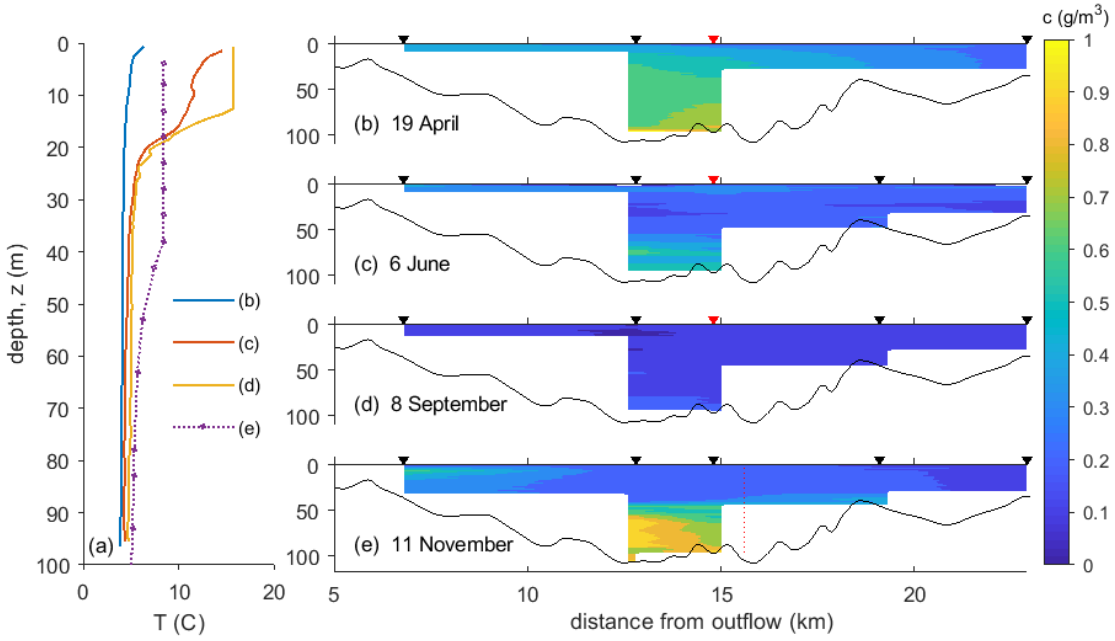

Figure 4.3: Seasonal stratification and sediment distribution during 2016 in the West Basin. (a) Temperature through depth at CTD station ST9 (note: the 11 November temperature profile uses thermistor data from mooring M3). (b-e) Contour plots of c through depth along the thalweg, with triangles showing where CTD stations are located. Red triangles (b-d) or dotted line (e) indicate where temperature profles shown in (a) were measured.

increasing each year at the onset of autumnal mixis.

The subsequent period of inverse stratification each winter brought a decrease in c and m (Hamilton et al., 2020; note that near the surface, this decrease is more pronounced under ice cover). Then, through each spring mixis, c and m increased to similar peak values as those observed during the preceeding autumnal mixis (Figure 4.2a,b). The long term trend in peak m through the seasonal regime saw lower maxima during autumn and spring mixis with each passing year. This study's final CTD transect, collected on 4 December 2018, showed m still above the historical maximum (Figure 4.2b). The trend indicates that this would also have been the case in spring 2019, but that in time seasonal fluctations in m will occur within the range of naturally occurring sediment mass.

The decaying trend we see in West Basin suspended sediment m during the seasonal regime tells us that sinks of suspended sediment were overcoming sources on an inter-annual basis, while the cyclical pattern in m tells us that sources were overcoming sinks during certain parts of the year. We now consider the role of each sink during the seasonal regime, starting with river flushing.

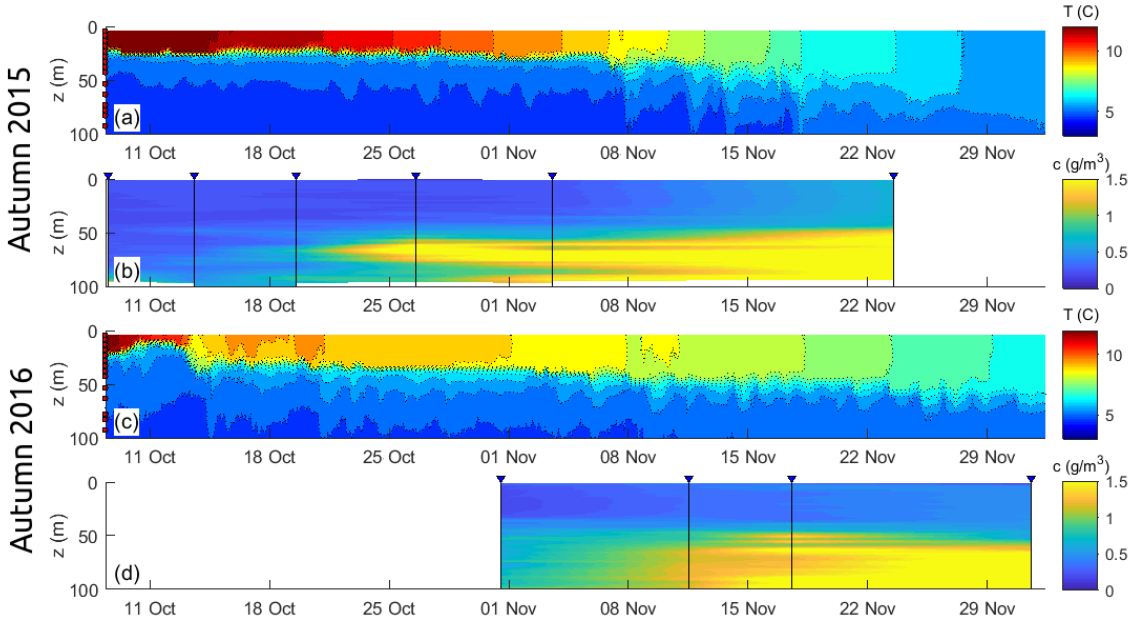

Figure 4.4: Autumn temperature (a,c) and suspended sediment (b,d) contour plots. Red dots to the left of (a) and (c) indicate thermistor depths on mooring M3, and blue triangles along the top of (b) and (d) indicate the timing of CTD transects. The last three CTD transects in (d) are shown in greater detail in Figure 4.5.

In the Quesnel River, sediment c followed the cyclical pattern of West Basin surface c through the seasonal regime (Figure 4.2d), ranging from lows of $c \approx 0.1$ g/m^3 during summer and winter stratified periods to highs of $c \approx 0.4$ g/m^3 at autumn and spring mixis. Both Q and $\dot{m}_r$ were highest during spring freshet (although still an order of magnitude smaller than peak levels seen in December 2014, during the initial regime), and peaked in either late May or early June of each year (the study period maximum $Q = 471$ m^3/s was recorded on 26 May 2018, which coincided with the seasonal cycle maximum $\dot{m}_r = 11 \pm 2$ Mg/day; Figure 4.2c). High river c also followed heavy precipitation early in autumn 2015 and 2016; these periods are indicated by increased river flow (Q), and result in elevated mass flow ($\dot{m}_r = 4.5 \pm 1$ Mg/day on 29 September 2016, Figure 4.2e). The least outflow of sediment through the river occurred during winter. This may seem unremarkable given that flow rates (Q, Figure 4.2c) reach their yearly minima, but there is another reason for why winter sediment flushing is so insubstantial.

Especially under ice cover, winter inverse stratification leads to a quiescent surface layer, and

these waters become exceptionally clear as sediment settles out. The surface turbidity sensor on mooring M3 has a nominal depth of 4 m, based on a yearly average. In midwinter, when the water level is at its lowest, this sensor can come to within 2 m of the surface. From mid-February until mid-March 2017, c was below its level of detection (Figure 4.2a), and bottle samples taken from the river had similarily low c (Figure 4.2d). Based on a particle settling velocity of $w_s = 5$ cm/day, near-total stillness under the ice could cause complete clarification to 2 m depth within 40 days. As we discuss next, seiche-driven resuspension and surface mixed layer deepening raised bottom sediment to the surface prior to each winter of 2015 to 2018. Much more of this sediment would have been flushed out of the basin by the river were it not for the settling that winter inverse stratification allowed for.

Flushing of suspended sediment by exchange flows between the West Basin and the main basin of Quesnel Lake is the other sink we must consider (we need not consider settling on an inter-annual basis, for reasons we will explain shortly). The strong concentration gradient found between the West Basin and the main basin of Quesnel Lake during the initial regime meant that the flow of sediment into the West Basin was negligible compared to the flow out. During the seasonal regime, however, this one-way assumption no longer holds. Because of the slow settling velocity of fine particles, a substantial mass of spill-related sediment would have remained in suspension in the main basin. Additionally, the main basin receives sediment from three large rivers (the Horsefly, Mitchell, and Niagara, described in Chapter 2), meaning that under natural conditions, the sediment c gradient would lead to a net flow of sediment into the West Basin (also the direction of the hydraulic gradient). Nonetheless, because river $\dot{m}_r$ decreases once the lake is stratified, the process of West Basin hypolimnetic flushing by exchange flow must account for most of the decrease in sediment m that we observe during stratified periods (Figure 4.2b). Having considered these sinks, we will finally consider sources of sediment.

Hamilton et al. (2020) showed that increased hypolimnetic suspended sediment c was associated with baroclinic seiching, something we will now explore in further detail as we discuss the bottom as a source of sediment. Previously, we considered mass flow across the bottom boundary ($\dot{m}_b$) in terms of settling to assess how much of the decrease in West Basin sediment m could be

attributed to $\dot{m}_b$ over the initial regime. During autumn of each year in the seasonal regime, $\dot{m}_b$ is more important as a source of sediment, through resuspension, than it is as a sink, through settling. Seiche motion has been shown to generate currents in lakes that can transport suspended sediment into the water column in two ways: from the bottom up, through turbulent mixing in the benthic boundary layer; and from the sides in, through intrusions (Gloor et al., 1994; Marti and Imberger, 2006; Wain and Rehmann, 2010). In summer 2016, a several centimeter-thick, cloudy, mobile layer was observed overlaying more consolidated material in cores taken from the spill-affected bottom region of the West Basin (Hamilton et al., 2020); this has been hypothesized to be the source of elevated hypolimnetic turbidity each autumn of 2015-2018. Strictly speaking, sediment in this layer is already in suspension; here the term "resuspension" is used to describe the movement of sediment out of this layer into the water column where it may be detected using a profiling or moored instrument.

To demonstrate the effect of seiche on West Basin c during the seasonal regime, Figure 4.4 shows temperature and c through depth and across time in the autumns of 2015 and 2016, while Figure 4.5 shows $c(z)$ profiles together with bottom current velocity from autumn 2016. As the surface mixed layer deepens and seiche amplitude increases, distinct layers of increased c appear in the lower half of the water column (Figure 4.4). CTD transects each autumn record these layers, often at multiple depths, and occasionally at coherent depths in neighbouring CTD stations ST9 and ST10. We show an example of these layers in profiles collected on 17 November 2016, at depths of around 55 and 62 m (Figure 4.5b). These spikes in suspended sediment c could indicate the horizontal transport of sediment by intrusions (cf. Wain and Rehmann, 2010), and they are stronger toward ST10, meaning that these two particular examples would have originated from the sloping bottom toward the northern (downstream) end of the West Basin.

As discussed in Chapters 1 and 2, sediment resuspension and bottom boundary mixing are different for sloping and flat bottom regions. In Lake Alpnach, Switzerland, Gloor et al. (1994) observed sediment resuspension over a flat bottom during bursts of current with velocities of up to 7 cm/s. Velocity data collected below 100 m depth at mooring TuADCP (Figure 1.1) during autumn 2016 showed horizontal velocities of up to 8.6 cm/s (recorded 5 m above bottom at 01:12

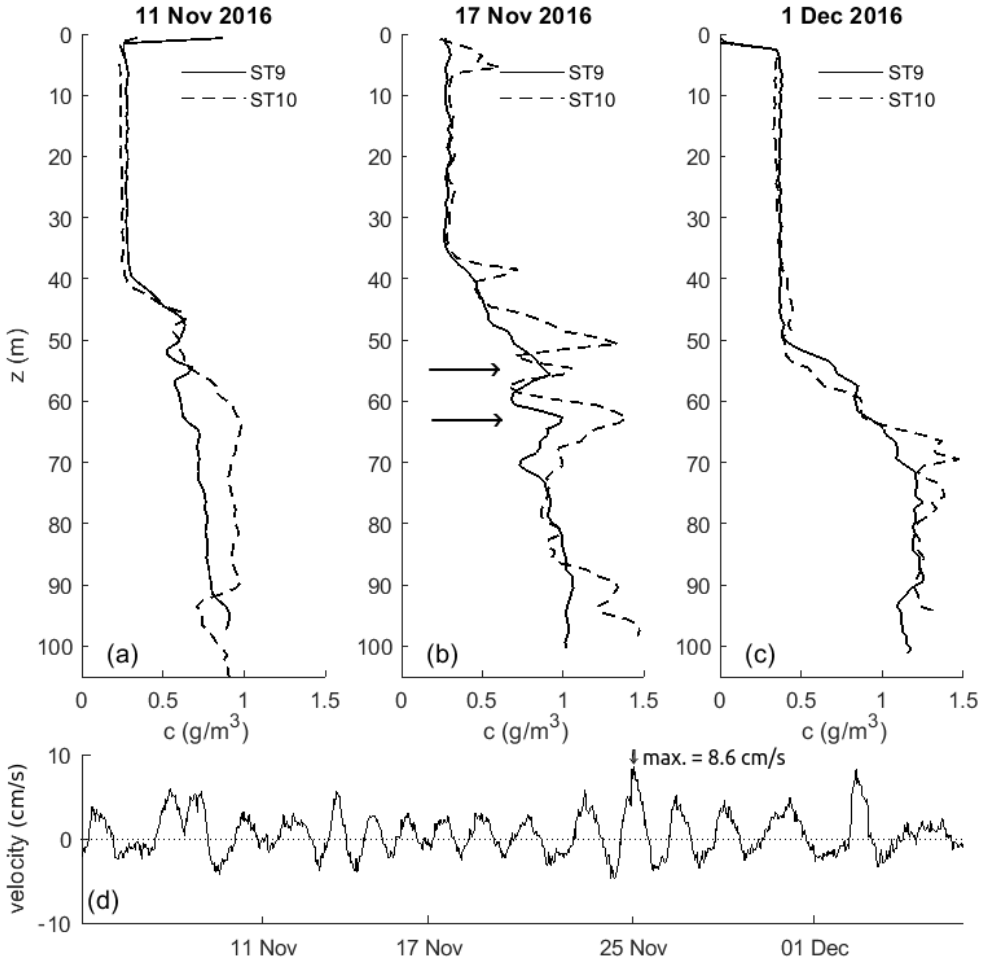

Figure 4.5: Autumn 2016 CTD (a,b,c) and ADCP (d) data, (a)-(c) compare *c* profiles at neighbouring stations ST9 and ST10, and (d) shows the along-thalweg horizontal current velocity measured 5 m above bottom at TuADCP.

on 25 November 2016; Figure 4.5d). The peak velocity for the period shown occurred between CTD transects on 17 November and 1 December 2016. What is interesting to note is that suspended sediment *m* does not appreciably increase between these two dates (Figure 4.2b). This could indicate that earlier in autumn 2016, the critical shear stress needed to remobilize unconsolidated bottom sediment had already been exceeded for a sufficient duration to raise sediment into the water column. Even higher horizontal current velocities were recorded in autumn 2017 (not shown), yet the West Basin's maximum observed sediment *m* that year was slightly lower than was observed in autumn 2016 (Figure 4.2b). It appears that seiche currents in the West Basin have been strong enough

to resuspend bottom sediment during each autumn of the seasonal regime, and that the decaying interannual trend we observe in sediment m could result from there being less sediment available to resuspend.

Aside from the periods of increasing m that we observed each fall, we also saw a slight increase in West Basin m toward the end of each period of winter inverse stratification as the lake approached spring mixis (typically around March of each year; Figure 4.2b). We attribute this increase partly to riverine sediment input: the $c(z)$ profile collected at CTD station ST9 on 6 June 2016 shows slightly elevated c between the surface and 20 m depth, indicative of a riverine overflow. Another potential source of sediment m during the breakdown of winter inverse stratification is remobilization of bottom sediment. Unfortunately, with limited spatial coverage of c during the winter months, we are unable to resolve this process to the same degree as we have done for the seiche-driven remobilization during the autumn.

A last, and lesser source of sediment is the pair of multi-port diffusers located around 50 m depth, 250 m offshore of Hazeltine Creek (described in section 1.1). Denoting their associated sediment mass flow as $\dot{m}_d$, we calculate an upper-range estimate using their permitted annual mean flow rate ($Q = 29000$ m^3/day) and maximum concentration ($c = 7$ g/m^3, actual c varies, and is typically below the permitted level; MPMC, 2018) to give $\dot{m}_d \approx 0.2$ Mg/day. This upper bound estimate is one to two orders of magintude smaller than the loading required to explain the increase in West Basin m during each autumn of 2015-2018.

Chapter 5

Discussion

Quesnel Lake is gradually returning toward its background level of naturally occurring suspended sediment. One aspect that is central to how the lake is recovering was that the 4 August 2014 flood entered the lake's smaller, downstream basin. Here we draw on theory for insight into how inter-basin flows, relative basin size, particle settling, and river flow broadly shaped the system's response. We begin with the case of one completely mixed basin; examining what would have happened if the spill had occurred during autumnal mixis into a lake the size and shape of the West Basin, with an outflow comparable to the Quesnel River, and an equally sized inflow.

The mathematical theory for such a problem is well formulated for continuously stirred tank reactors (CSTRs, cf. Chapra, 1997). If the flow (Q) that enters a CSTR has zero suspended sediment concentration (c_d), the sediment mass balance is given by:

$$\frac{dm}{dt} = V_d \frac{dc_d}{dt} = -Qc_d - w_s A_d c_d, \tag{5.1}$$

where A_d is lake surface area, V_d is volume (constant with inflow equal to outflow), and w_s is particle settling velocity. Here time is the independent variable, and concentration is the dependent variable for which we solve an initial value problem to obtain an expression for $c_d(t)$. Grouping constant

terms (with $V_d/A_d = H_d$, average depth), we have:

$$\frac{dc_d}{dt} = -\left(\frac{Q}{V_d} + \frac{w_s}{H_d}\right) c_d = -\lambda c_d, \tag{5.2}$$

which for an initial concentration $c_d(0) = c_i$ has a solution:

$$c_d(t) = c_i e^{-\lambda t}. \tag{5.3}$$

The exponential term λ is the decay constant; its inverse is the e-folding time, for 63% removal ($1 - e^{-1} \approx 0.63$) of mass. For dissolved matter, equation (5.2) retains the flushing term (Q/V_d) but not the settling term (w_s/H_d), and provided the substance is not removed by chemical reactions, its e-folding time will be the basin's residence time ($t_r = V_d/Q = 1$ km^3/100 m^3/s ≈ 100 days). This also applies to 1 μm diameter particles that settle at 5 cm/day in a basin with an average depth of $H_d = 42$ m (that of the West Basin), as w_s/H in this case is two orders of magnitude smaller than Q/V_d.

Compared to this one basin case, we see a much higher flushing rate in the West Basin through autumnal mixis of 2014. Fitting an exponential decay curve to the mass time series over this period gives an e-folding time of about 50 days, half that of the one basin case. By extension, half of the flushing may be attributed to the river; indeed, observed river mass flow ($\dot{m}_r$) in early December 2014 is roughly half that of the observed rate of decrease in the West Basin. The settling $\dot{m}_b$ we estimate for this period in section 4.1 is one order of magnitude smaller than $\dot{m}_r$. Although this a lesser disparity than the two orders of magnitude given by equation (5.2), it still suggests that mass flow eastward over the Cariboo Island sill was comparable to mass flow down the Quesnel River at this time.

Using this result, we will extend the CSTR theory to a two basin system with constant, bi-directional exchange flow (Q_x) equal in magnitude to river flow ($Q_r = 131$ m^3/s). As with Quesnel Lake, we will consider the case of an upstream basin (denoted with the subscript u) with greater volume ($V_u = 40.8$ km^3, $V_d = 1$ km^3) and surface area ($A_u = 243$ km^2, $A_d = 23$ km^2). The schematic in Figure 5.1b depicts the transport terms that apply to each basin, also given in equations (5.6)-

(5.9). The mass balance for each basin is affected by its own concentration as well as that of the other basin, yielding a system of two linear, homogeneous, ordinary differential equations:

$$\frac{dc_u}{dt} = -\alpha_{uu}c_u + \alpha_{ud}c_d, \tag{5.4}$$

$$\frac{dc_d}{dt} = \alpha_{du}c_u - \alpha_{dd}c_d, \tag{5.5}$$

with coefficients (α) given by the transport terms:

$$\alpha_{uu} = \frac{Q_r + Q_x}{V_u} + \frac{w_s}{H_u}, \tag{5.6}$$

$$\alpha_{ud} = \frac{Q_x}{V_u}, \tag{5.7}$$

$$\alpha_{du} = \frac{Q_r + Q_x}{V_d}, \text{ and} \tag{5.8}$$

$$\alpha_{dd} = \frac{Q_r + Q_x}{V_d} + \frac{w_s}{H_d}. \tag{5.9}$$

The general solution to this two basin system has the form:

$$\begin{bmatrix} c_u(t) \\ c_d(t) \end{bmatrix} = \mathbf{c}(t) = k_f e^{\lambda_f t}\eta_f + k_s e^{\lambda_s t}\eta_s, \tag{5.10}$$

with two decay terms, denoted by the subscripts f and s, corresponding to fast and slow response. As with the two regimes observed in the West Basin following the spill, the solution predicts an initial period of rapidly decreasing c transitioning into a slow, sustained decrease. The decay constants for these two regimes are the eigenvalues λ_f and λ_s, given by:

$$\lambda_{f,s} = \frac{-(\alpha_{uu} + \alpha_{dd}) \pm \sqrt{(\alpha_{uu} + \alpha_{dd})^2 - 4(\alpha_{uu}\alpha_{dd} - \alpha_{ud}\alpha_{du})}}{2}. \tag{5.11}$$

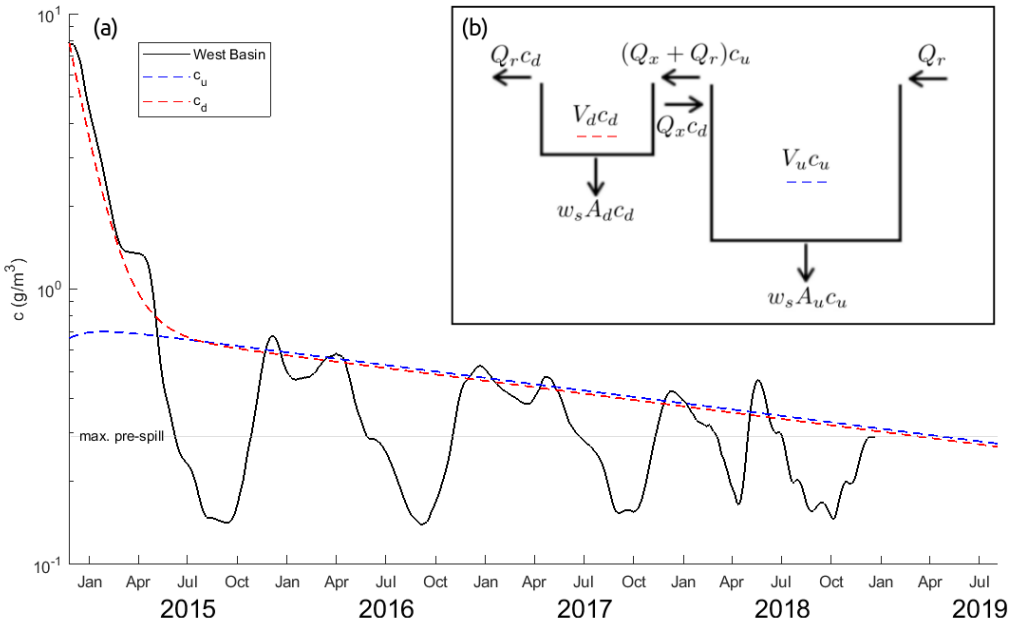

Figure 5.1: Two basin system: (a) compares the analytical solution, given by equations (5.10)-(5.12), to the volumetric average of West Basin suspended sediment concentration; and (b) depicts the transport terms for the upstream and downstream basin mass balances. The y-axis intercept is at 0.1 g/m^3, which is slightly higher than the approximate median pre-spill c =0.08 g/m^3.

The relative weighting of each basin's role in the fast and slow regimes is given by the fast and slow eigenvectors η_f and η_s, as:

$$\eta_{f,s} = \begin{bmatrix} \alpha_{ud} \\ \alpha_{uu} + \lambda_{f,s} \end{bmatrix} = \begin{bmatrix} \alpha_{dd} + \lambda_{f,s} \\ \alpha_{du} \end{bmatrix}. \tag{5.12}$$

Having calculated $\lambda_{f,s}$ and $\eta_{f,s}$, one specifies the initial concentrations of the upstream and downstream basins to determine the constants k_f and k_s in equation (5.10). For the present case, we initilize the model at the onset of autumnal mixis 2014 in the West Basin (22 November= $t(0)$). We take $c_u(0) = 0.7$ g/m^3 (roughly, the decrease in West Basin m between 10 September and 22 November 2014, which was 30000 Mg, less the cumulative river and settling mass flows, which were 800 and 2300 Mg, respectively, divided by V_u), and $c_d(0) = 8$ g/m^3 (the remaining mass suspended in the West Basin, which was 8000 Mg, divided by V_d). For this completely mixed, two

basin model, we also assume the sediment remaining in suspension had the Stokes' velocity of 1 μm particles ($w_s = 5$ cm/day; section 3.3).

The particular solution to this two basin, analytical model is plotted in Figure 5.1, along with West Basin c from mass data (Figure 4.2b). To remove the oscillatory effect of seiche on West Basin c in Figure 5.1, we smooth m with a 21 day moving average before dividing by V_d. Because the model uses constant transport terms, it cannot capture the seasonality of the real system. Nonetheless, three key aspects of the real system are reflected in the model: the decay rate of the initial regime (given by the eigenvalue λ_f); the timing of the transition between regimes; and the decay rate of the seasonal regime (given by λ_s). All three of these are inherent to the modelled system (i.e. independent of initial concentrations). Initially, the fast term in equation (5.10) dominates decay of c_d; this results from the coefficient α_{dd} being two orders of magnitude larger than α_{uu}, α_{ud}, and α_{du}, meaning that c_d is controlled by the combined flushing from river and exchange flows between the two basins. Later, during slow decay, both c_d and c_u are controlled mainly by the upstream basin due to its larger volume and surface area. Whereas the settling term in the coefficient α_{dd} is insignificant, for α_{uu} it is on the same order as the flushing term, giving a slow decay e-folding time of about 5 years (half the residence time of Quesnel Lake). The similarity between the two basin model's slow decay and the observed inter-annual trend could suggest that the whole of Quesnel Lake is recovering from the spill, rather than its effects having been confined to the West Basin. By altering $c_u(0)$ and/or $c_d(0)$, we can adjust the long term decay trend to match the peak c observed each autumn in the West Basin. Our interest is in finding the time at which the modelled c_d will be equal to the pre-spill median ($c \approx 0.08$ g/m^3), so that we may assess how long it will take for Quesnel Lake to return to its naturally occurring sediment load. Doing so, we find this time to be approximately one decade.

A problem that arises in using a completely mixed model to describe a seasonally stratified system is that the model will overpredict river mass flow, because river c during stratified periods tends to be lower than surface c. The model's completely mixed assumption holds during periods of autumnal and vernal mixis (grey-shaded timespans indicated in Figure 4.2). At those times, which make up less than a quarter of a given year, river c is approximately the volumetric average

West Basin c. During stratified periods (most of the year), c near the surface of the West Basin, and consquently in the river, are lower than the volumetric average (most sediment mass is in the hypolimnion). In the particular solution shown in Figure 5.1, between 22 November 2014 and 21 December 2018, the model gives cumulative river mass flow $\approx$ 10000 Mg, twice that observed in the Quesnel River over this period (based on data shown in Figure 4.2e). Although the model provides a broad description of Quesnel Lake's two-phased response to the slug injection of suspended sediment following the the Mount Polley spill, it is not a replacement for data when assessing the actual mass flows of suspended sediment out of the West Basin.

Note that during each of the summer stratified periods of 2015-2018, the rate of West Basin c decrease is similar to the fast decay predicted for c_d in the model. The completely mixed model's fast decay results from both river and inter-basin flushing, whereas in the real, stratified West Basin, the river draws water (and suspended sediment) only from the surface mixed layer. In their study of late summer upwelling in Quesnel Lake, Laval et al. (2008) estimated a residence time of 6-8 weeks for the West Basin hypolimnion based on observed changes in heat content. Upwelling occurs when the hypolimnion is brought to the surface by a tilted thermocline; it is associated with large seiche amplitudes, which the West Basin experiences because it is located at the extreme end of Quesnel Lake's long axis. Since c is typically higher in the hypolimnion (Figures 4.2a and 4.3b), the rate at which suspended sediment is flushed from the West Basin during the summer stratified period depends heavily on the exchange flows driven by seiche.

Chapter 6

Conclusions

Of the 38000 $\pm$ 11000 Mg of sediment that was in suspension below 30 m depth in Quesnel Lake's West Basin on 10 September 2014, $<$200 Mg remained in the water column by August 2015, one year post-spill. Most ($\sim$80%) of that mass exited east over the Cariboo Island sill during an initial, post-spill regime of sustained, rapid decay that lasted until early June of 2015. Of the $\sim$7000 Mg of sediment that flowed down the Quesnel River during the four year study, one third did so during the first autumn post-spill, and another sixth during the first winter. In the ensuing years, a seasonal pattern in West Basin sediment mass emerged: late summer yearly minima; loading from remobilization of bottom sediments during the breakdown of stratification leading to autumnal mixis maxima; decrease to winter local minima during inverse stratification; increase due to riverine and bottom sediment input to spring mixis maxima; and decrease following the onset of stratification. The autumn and spring maxima of this seasonal regime show an overall decreasing trend.

Consistent with the two regimes we observed in the West Basin, the analytical solution to a mass balance model for a system of two, completely mixed basins with constant exchange flow between basins and constant river flow predicts an initial, fast decay and a long-term, slow decay. This solution overpredicts mass flow in the river, but nevertheless gives two decay rates which reflect the observed decay rates of each regime and the timing of the transition from fast to slow decay of sediment concentration. Fitting the slow decay curve of the model to the autumnal maxima of West Basin sediment mass, and determining the point in time at which this curve crosses the pre-spill

median mass, we find that Quesnel Lake will return to pre-spill levels of suspended sediment within approximately one decade of the 4 August 2014 spill.

Bibliography

V. Axelsson. The Laitaure Delta: A study of deltaic morphology and processes. *Geografiska Annaler. Series A, Physical Geography*, 49(1):1, 1967. doi:10.2307/520865. → page 7

J. Bloesch. Mechanisms, measurement and importance of sediment resuspension in lakes. *Marine and Freshwater Research*, 46:295–304, 1995. doi:10.1071/MF9950295. URL http://www.publish.csiro.au/mf/MF9950295. → pages 1, 9

E. C. Carmack, C. B. J. Gray, C. H. Pharo, and R. J. Daley. Importance of lake-river interaction on seasonal patterns in the general circulation of Kamloops Lake, British Columbia. *Limnology and Oceanography*, 24(4):634–644, 1979. doi:10.4319/lo.1979.24.4.0634. → page 7

S. C. Chapra. *Surface Water Quality Monitoring*. McGraw-Hill, Toronto, 1997. → pages 2, 6, 8, 9, 37

M. R. Chowdhury, M. G. Wells, and T. Howell. Movements of the thermocline lead to high variability in benthic mixing in the nearshore of a large lake. *Water Resources Research*, 52(4): 3019–3039, 2016. doi:10.1002/2015WR017725. URL https://agupubs.onlinelibrary.wiley.com/doi/abs/10.1002/2015WR017725. → pages 2, 8

K. L. Deines. Backscatter estimation using broadband acoustic Doppler current profilers. In *Proceedings of the IEEE Sixth Working Conference on Current Measurement*, pages 249–253, Sand Diego, CA, March 1999. → page 16

H. B. Fischer, E. J. List, R. C. Koh, J. Imberger, and N. H. Brooks. Chapter 6 - mixing in reservoirs. In H. B. Fischer, E. J. List, R. C. Koh, J. Imberger, and N. H. Brooks, editors, *Mixing in Inland and Coastal Waters*, pages 148 – 228. Academic Press, San Diego, 1979. ISBN 978-0-08-051177-1. doi:https://doi.org/10.1016/B978-0-08-051177-1.50010-6. URL http://www.sciencedirect.com/science/article/pii/B9780080511771500106. → page 9

R. E. Francois and G. R. Garrison. Sound absorption based on ocean measurements: Part I: Pure water and magnesium sulfate contributions. *Journal of the Acoustical Society of America*, 72(3): 896–907, 1982. → page 16

J. W. Gartner. Estimating suspended solids concentrations from backscatter intensity measured by acoustic Doppler current profiler in San Francisco Bay, California. *Marine Geology*, 211(3-4): 169–187, 2004. doi:10.1016/j.margeo.2004.07.001. → page 16

R. Gilbert and J. R. Desloges. Late glacial and Holocene sedimentary environments of Quesnel Lake, British Columbia. *Geomorphology*, 179:186 – 196, 2012. ISSN 0169-555X.

doi:https://doi.org/10.1016/j.geomorph.2012.08.010. URL http://www.sciencedirect.com/science/article/pii/S0169555X12004011. → pages 3, 8, 10

M. Gloor, A. Wüest, and M. Münnich. Benthic boundary mixing and resuspension induced by internal seiches. *Hydrobiologia*, 284(1):59–68, May 1994. ISSN 1573-5117. doi:10.1007/BF00005731. URL https://doi.org/10.1007/BF00005731. → pages 1, 9, 23, 34

M. Gloor, A. Wüest, and D. M. Imboden. Dynamics of mixed bottom boundary layers and its implications for diapycnal transport in a stratified, natural water basin. *Journal of Geophysical Research: Oceans*, 105(C4):8629–8646, 2000. doi:10.1029/1999jc900303. → page 1

Golder Associates Ltd. Mount Polley Mining Corporation post-event environmental impact assessment report - key findings report. Technical report, Golder Associates Ltd., 2015. URL https://www.imperialmetals.com/assets/docs/mt-polley/2015-06-18-MPMC-KFR.pdf. → page 11

A. K. Hamilton, B. E. Laval, E. L. Petticrew, S. J. Albers, M. Allchin, S. A. Baldwin, E. C. Carmack, S. J. Déry, T. D. French, B. Granger, K. E. Graves, P. N. Owens, D. T. Selbie, and S. Vagle. Impacts of the 2014 Mount Polley mine tailings dam breach on the physical limnology of Quesnel Lake, Canada: baseline to three years post-spill. *Water Resources Research (in publication)*, 2020. → pages 2, 6, 8, 12, 19, 24, 26, 30, 31, 33, 34

I. Hatam, E. L. Petticrew, T. D. French, P. N. Owens, B. Laval, and S. A. Baldwin. The bacterial community of Quesnel Lake sediments impacted by a catastrophic mine tailings spill differ in composition from those at undisturbed locations – two years post-spill. *Scientific Reports*, 9 (2705):1 – 11, 2019. doi:https://doi.org/10.1038/s41598-019-38909-9. URL https://www.nature.com/articles/s41598-019-38909-9.pdf. → page 18

L. Håkanson and M. Jansson. *Principles of Lake Sedimentology*. Springer, New York, 1983. → pages 1, 6, 7, 8, 23

B. E. Laval, J. Morrison, D. J. Potts, E. C. Carmack, S. Vagle, C. James, F. A. McLaughlin, and M. Foreman. Wind-driven summertime upwelling in a fjord-type lake and its impact on downstream river conditions: Quesnel Lake and River, British Columbia, Canada. *Journal of Great Lakes Research*, 34(1):189 – 203, 2008. ISSN 0380-1330. doi:https://doi.org/10.3394/0380-1330(2008)34[189:WSUIAF]2.0.CO;2. URL http://www.sciencedirect.com/science/article/pii/S0380133008700157. → pages 10, 42

B. E. Laval, S. Vagle, D. Potts, J. Morrison, G. Sentlinger, C. James, F. McLaughlin, and E. C. Carmack. The joint effects of riverine, thermal, and wind forcing on a temperate fjord lake: Quesnel Lake, Canada. *Journal of Great Lakes Research*, 38(3):540 – 549, 2012. ISSN 0380-1330. doi:https://doi.org/10.1016/j.jglr.2012.06.007. URL http://www.sciencedirect.com/science/article/pii/S0380133012001323. → page 3

G. A. Lawrence, J. M. Burke, T. P. Murphy, and E. E. Prepas. Exchange of water and oxygen between the two basins of Amisk Lake. *Canadian Journal of Fisheries and Aquatic Sciences*, 54 (9):2121–2132, 1997. doi:10.1139/f97-235. URL https://doi.org/10.1139/f97-235. → pages 2, 10

P. C. Manins. Intrusion into a stratified fluid. *Journal of Fluid Mechanics*, 74(3):547–560, 1976. doi:10.1017/S0022112076001948. → page 29

C. L. Marti and J. Imberger. Dynamics of the benthic boundary layer in a strongly forced stratified lake. *Hydrobiologia*, 568(1):217–233, 09 2006. URL http://ezproxy.library.ubc.ca/login?url=https://search.proquest.com/docview/821258229?accountid=14656. Copyright - Springer 2006; Last updated - 2014-08-16. → pages 2, 9, 29, 34

A. J. Mehta. *An introduction to hydraulics of fine sediment transport*. World scientific, 2014. → page 6

MPMC. Post-event environmental impact assessment report, June 2015. URL http://www2.gov.bc.ca/assets/download/DD7C810289EE434A9E88C682556B6D45. → pages 2, 3, 18

MPMC. 2018 annual discharge plan, July 2018. URL https://j200.gov.bc.ca/pub/ams/download.aspx?PosseObjectId=105984433. → pages 5, 36

E. L. Petticrew, S. J. Albers, S. A. Baldwin, E. C. Carmack, S. J. Déry, N. Gantner, K. E. Graves, B. Laval, J. Morrison, P. N. Owens, D. T. Selbie, and S. Vagle. The impact of a catastrophic mine tailings impoundment spill into one of North America's largest fjord lakes: Quesnel Lake, British Columbia, Canada. *Geophysical Research Letters*, 42(9):3347–3355, 2015. doi:10.1002/2015GL063345. URL https://agupubs.onlinelibrary.wiley.com/doi/abs/10.1002/2015GL063345. → pages 2, 6, 11, 12, 19, 22, 25, 26, 28

C. H. Pharo and E. C. Carmack. Sedimentation processes in a short residence-time intermontane lake, Kamloops Lake, British Columbia. *Sedimentology*, 26(4):523–541, 1979. doi:10.1111/j.1365-3091.1979.tb00927.x. → page 7

K. R. Scheu, D. A. Fong, S. G. Monismith, and O. B. Fringer. Sediment transport dynamics near a river inflow in a large alpine lake. *Limnology and Oceanography*, 60(4):1195–1211, 2015. doi:10.1002/lno.10089. URL https://aslopubs.onlinelibrary.wiley.com/doi/abs/10.1002/lno.10089. → pages 1, 7, 8, 23, 29

D. W. Schindler and J. R. Vallentyne. *Algal bowl: overfertilization of the worlds freshwaters and estuaries*. Earthscan, 2008. → page 1

Seapoint. Seapoint turbidity meter user manual, July 2013. URL http://www.seapoint.com/pdf/stm_um.pdf. → page 21

Tetra Tech EBA. Quesnel Lake water column observations and modelling. Technical report, Tetra Tech EBA, May 2015. → page 2

R. Valipour, L. Boegman, D. Bouffard, and Y. R. Rao. Sediment resuspension mechanisms and their contributions to high-turbidity events in a large lake. *Limnology and Oceanography*, 62(3): 1045–1065, 2017. doi:10.1002/lno.10485. URL https://aslopubs.onlinelibrary.wiley.com/doi/abs/10.1002/lno.10485. → page 1

D. J. Wain and C. R. Rehmann. Transport by an intrusion generated by boundary mixing in a lake. *Water Resources Research*, 46(8), 2010. URL http://ezproxy.library.ubc.ca/login?url=https://search.proquest.com/docview/860349282?accountid=14656. Copyright - Copyright 2010 by American Geophysical Union; Last updated - 2014-08-16. → pages 2, 9, 34

R. G. Wetzel. 21 - sediments and microflora. In R. G. WETZEL, editor, *Limnology (Third Edition)*, pages 631 – 664. Academic Press, San Diego, third edition edition, 2001a. ISBN 978-0-12-744760-5. doi:https://doi.org/10.1016/B978-0-08-057439-4.50025-3. URL http://www.sciencedirect.com/science/article/pii/B9780080574394500253. → page 1

R. G. Wetzel. 5 - light in inland waters. In R. G. WETZEL, editor, *Limnology (Third Edition)*, pages 49 – 69. Academic Press, San Diego, third edition edition, 2001b. ISBN 978-0-12-744760-5. doi:https://doi.org/10.1016/B978-0-08-057439-4.50009-5. URL http://www.sciencedirect.com/science/article/pii/B9780080574394500095. → page 1

R. G. Wetzel. 7 - water movements. In R. G. WETZEL, editor, *Limnology (Third Edition)*, pages 93 – 128. Academic Press, San Diego, third edition edition, 2001c. ISBN 978-0-12-744760-5. doi:https://doi.org/10.1016/B978-0-08-057439-4.50009-5. URL http://www.sciencedirect.com/science/article/pii/B9780080574394500095. → page 9

A. Wüest, G. Piepke, and D. C. V. Senden. Turbulent kinetic energy balance as a tool for estimating vertical diffusivity in wind-forced stratified waters. *Limnology and Oceanography*, 45(6):1388–1400, 2000. ISSN 00243590. URL http://www.jstor.org/stable/2670531. → page 1